Contents list available at IJRED website

International Journal of Renewable Energy Development

Journal homepage: https://ijred.undip.ac.id

Research Article

Predictive accuracy and characterisation of bio-oil yield from pyrolysis of *Cocos nucifera*: A comparison of traditional RSM and hybrid models

Anthony O. Onokwai[a,b*], Udochukwu B. Akuru[c], Dawood A. Desai[a]

[a]*Department of Mechanical and Mechatronics Engineering, Tshwane University of Technology, Pretoria 0183, South Africa*

[b]*Department of Mechanical Engineering, Pan-Atlantic University, Lekki, 105101, Nigeria*

[c]*Department of Electrical Engineering, Tshwane University of Technology, Pretoria 0183, South Africa*

Abstract. The pressing demand for renewable energy has made biomass a quintessential alternative to fossil fuels. This study aims to develop and compare predictive models for optimising bio-oil yield from the intermediate pyrolysis of Cocos nucifera, utilising response surface methodology with the central composite design and hybrid models (PSO-ANFIS and GA-ANFIS). It seeks to characterize the bio-oil yield to investigate its quality for use as a biofuel. An experimental run was performed by varying pyrolysis operating parameters, namely, temperature (300–700°C), heating rate (6–30°C/min), residence time (5–25 minutes), particle size (0.5–4.5 mm), and nitrogen flow rate (10–50 mL/min). Hybrid models (PSO-ANFIS and ANFIS-GA) were used to predict the bio-oil yield to identify the most robust model. An optimum bio-oil yield (52.17 wt.%) was attained at a temperature, heating rate, residence time, particle size, and nitrogen flow rate of 510.2°C, 10.5°C/min, 5.2 minutes, 0.3 mm, and 17.3 mL/min, respectively. The study shows that its hybrid models are scalable and outperform traditional techniques (RSM) in terms of predictive accuracy and computational efficiency. The GC-MS analysis identified over 200 compounds in bio-oil, comprising mainly phenols, esters, and oleic acids, which confirmed its suitability for producing biofuels, lubricants, and pharmaceuticals. Also, FTIR analysis confirms functional groups of biodiesel, adhesives, and resins. The PSO-ANFIS and GA-ANFIS models accurately predict the bio-oil yield, with the PSO-ANFIS model outperforming the other models with an R^2 of 0.994 and RMSE of 0.449 during the test phase, representing a two- to three-fold improvement over traditional RSM. Unlike conventional empirical models, the hybrid approach improves predictive accuracy and reduces the number of required experiments and computational errors, enabling real-time adjustments to the pyrolysis process, thereby advancing pyrolysis research and bio-oil optimization. This research is highly relevant for improving waste-to-energy production in regions where Cocos nucifera residues remain abundant, especially in emerging economies.

Keywords: Biofuels, Biomass, Characterization, Intermediate pyrolysis, Response Surface Methodology, Hybrid Models

Received: 9th March 2025; Revised: 7th May 2025; Accepted: 18th May 2025; Available online: 17th Sept 2025

1. Introduction

The increasing demand for renewable energy sources has placed biomass as one of the most relevant alternatives to fossil fuels (Onokwai *et al.*, 2022). Biomass, generated from agricultural residues, forestry waste, or dedicated energy crops, can be converted directly into biofuels, heat, and electricity (Garg *et al.*,2024). Among the different ways of conversion, pyrolysis is viewed as one of the most outstanding thermochemical procedures. Pyrolysis is a thermal decomposition (300–700°C) of organic material in an oxygen-free environment, producing bio-oil, biochar, and non-condensable gases (NCGs) (Yi *et al.*, 2023). Slow pyrolysis, which is characterized by low temperature operation and long residence time, generates the most biochar that can be used for carbon storage and to improve soil fertility. Fast pyrolysis gives importance to rapid heating and short residence time, increasing the yield of bio-oil(Prasetiawan *et al* 2023) . Heating rates in flash pyrolysis are even faster, requiring advanced systems and processes strictly controlled (Huang *et al.*, 2023). Intermediate pyrolysis is generally conducted at moderate temperatures (350-550°C) with short vapour residence times (10-30 minutes), with balances of bio-oil yield and quality (Olayokun *et al.*, 2024). The bio-oil yield, with less oxygenates, is more stable for fuel use and industrial applications, while biochar still retains high carbon content and porosity, making it suitable for agricultural and environmental uses (Xu *et al.*, 2020).

Coconut shell (*Cocos nucifera*) is considered an excellent biomass feedstock for intermediate pyrolysis in countries such as Nigeria (Tabal *et al.*, 2023). These coconut wastes are underutilized or even disposed of with hazardous methods such as open burning, which could instead be converted to bio-oil and biochar using intermediate pyrolysis; thus, addressing the problem of their waste management, besides encouraging renewable energy production (Azeta *et al.*, 2021). Therefore, it adds to sustainable development and the reduction of environmental pollution. Optimizing the operational parameters and conditions of the intermediate pyrolysis is vital for a high yield and to improve the quality of the products. The parameters are related to each other in a very complicated nonlinear way, including temperature, heating rate, residence time, particle size, and nitrogen flow rate (Mian *et al.*, 2024).

* Corresponding author
Email: onokwaiao@tut.ac.za (A.O.Onokwai)

https://doi.org/10.14710/ijre2025.61190
ISSN: 2252-4940/© 2025.The Author(s). Published by CBIORE

Response surface methodology (RSM) optimises various processes by modelling and quantifying the relationships between operating parameters and response variables (Vellaiyan *et al*., 2024). RSM, with the help of experimental designs such as Central Composite Design (CCD), optimises efficiency by minimizing runs of experiments so that the results obtained are accurate yet resource-efficient (Kundu *et al*., 2024). Numerous empirical studies substantiate the optimality of RSM in the pyrolysis process. (Nawaz *et al*., 2024), applied RSM intending to optimise macadamia nutshell pyrolysis and showed better bio-oil yield as a result of the interaction of several parameters like temperature, heating rate, and nitrogen flow rate. Similarly, (Hasan *et al*., 2023) conducted RSM on the pyrolysis experiments of sugarcane bagasse and demonstrated its potential to yield a very good prediction with a minimum number of efforts to maximize yields. (Chen *et al*., 2024) utilized RSM through CCD to optimise bio-oil yield from PKS pyrolysis and reported an optimal condition that yielded 47.10 wt.% bio-oil. These studies depict the use of RSM in improving the efficiency of pyrolysis and bio-oil production. In the pyrolysis experiment in an inert atmosphere, (Okokpujie *et al*., 2023) carried out RSM to optimise bio-oil yield. The study demonstrates that bio-oil production depends on reaction temperature, heating rates, and reaction time. This research produced bio-oil of 47.10 wt% at 520 °C, which exceeded existing fast pyrolysis yield records. FTIR and GC-MS analysis of the bio-oil composition indicates its applicability in diesel engines as well as marine equipment and industrial processes, which demonstrates PKS's potential as a viable alternative fuel. (Rahimi *et al*., 2023) applied the machine learning (ML) models to predict and optimise biofuel yields of biomass pyrolysis using walnut shells and seed cake as feedstocks. Seven ML models showed high predictive accuracy (R^2 = 0.95–0.99), and the best performance of the radial basis function. Genetic algorithms (GA) combined with Radial Basis Function (RBF) gave optimum yields of 36.04 wt.% for biochar, 45 wt.% for bio-oil, and 54.16 wt.% for NCGs. The sensitivity analysis showed that the biomass species and pyrolysis conditions were the most important parameters. However, the reliance on certain biomass types and respective experimental datasets may limit generalization to other feedstocks and diverse pyrolysis systems without further validation. Nevertheless, ML techniques, particularly Adaptive Neuro-Fuzzy Inference Systems (ANFIS), handle nonlinearities and complexities of the pyrolysis processes (Tang *et al*., 2024). ANFIS allows the modelling of complex relations between operating parameters and pyrolysis outcomes by incorporating pattern recognition capabilities of artificial neural networks (ANNs) with interpretability provided by fuzzy logic (FL). Besides, the performance of the ANFIS models could be improved further by using metaheuristic algorithms such as Particle Swarm Optimization (PSO) and GA, as stated by Jabeen *et al.* (2023).

PSO-ANFIS utilizes swarm intelligence to optimise fuzzy membership functions and model parameters. Particles iteratively explore the search space for efficient convergence toward optimal solutions and show superiority in predicting bio-oil and biochar yields by capturing complex nonlinear interactions at play (Li *et al*., 2021; Salameh *et al*., 2022). In the case of GA-ANFIS, evolutionary strategies such as selection, crossover, and mutation prevent early convergence and help in optimizing the parameters for reliable results even in multimodal spaces (Chen *et al*., 2024; Tumuluru & Heikkila, 2019). (Haq *et al*., 2022) incorporated ML with GA and PSO for biochar yield prediction and proposed the ELT-PSO model, which had a very high accuracy of R^2 = 0.99 and RMSE = 2.33. The software tool developed using ELT-PSO can predict the yields with an error margin of 2%, but it has its application is limited to biochar only. (Li *et al*., 2021) proposed an ANFIS model for bio-oil yield optimization, which was further optimised using GA and PSO, based on 244 historical data. PSO-ANFIS outperformed GA-ANFIS with R^2 = 0.968 and RMSE = 1.4443; however, the dependence on biomass type and specific pyrolysis conditions reduces versatility. (Azizi *et al*., 2024) utilised an ANFIS optimised with PSO to predict biochar yield from biomass pyrolysis. This approach overcomes limitations of least square support vector machines with respect to local optima and high time complexity. The key input parameters are heating rate, pyrolysis temperature, moisture content, holding time, and sample mass, while the outputs are biochar mass and yield. In addition, the ANFIS model outperformed the existing methods in terms of performance metrics: root mean square error (0.2673), coefficient of determination (0.9842), and average absolute percent relative error (3.4529). However, the model's reliance on accurate training data may limit its applicability to broader biomass types and conditions.

Despite the use of metaheuristic optimization algorithms such as ANFIS, ANFIS with GA, and ANFIS with PSO for the intermediary pyrolysis process, the consideration of more than three operating parameters, such as temperature, heating rates, residence time, particle size, nitrogen flow rate, and pyrolysis conditions, has not been comprehensively reported. Many researchers have looked into the use of coconut shells as biomass feedstock for pyrolysis because of their high lignin content and the possibility of producing bio-oil from them (Ahmad *et al*., 2021; Azeta *et al*., 2021; Ratnasari *et al*., 2024). Different methods have been tried in the past, including RSM and ANN optimizations, to improve bio-oil yield, and the ANFIS bio-oil yield prediction model (Agu *et al*., 2024; Li *et al*., 2021; Mathur *et al*., 2023). However, numerous such studies have flaws that restrict their usefulness in real-world applications. One limitation includes multiple parameters optimisation, as most of the previous studies tend to optimize a few parameters, mostly temperature, heating rate, nitrogen flow rate, and ignore the more complex problems of multi-parameter interactions. Besides, conventional RSM models fail to accurately describe the nonlinearities relationships of many pyrolysis processes, which makes the predictions less reliable. Also, some studies use machine learning models in isolation without hybrid techniques, which reduces their robustness in process optimization. Also, most of the previous models are less applicable due to their inability to provide real-time control, which is critical for large-scale processes (Kaur *et al*., 2024; Ikpeseni *et al*., 2024; Nawaz *et al*., 2024; Huraira *et al*., 2023; Mathur *et al*., 2023; Chhikara *et al*., 2023; Abatyough *et al*., 2022; Li *et al*., 2021; Chukwuneke *et al*., 2022; Laougé *et al*., 2020; Chan *et al*., 2017; Sareekam *et al*., 2016).

The current study intends to fill this knowledge gap by integrating RSM with hybrid artificial intelligence-based models (PSO-ANFIS and GA-ANFIS), adopting five parameters simultaneously to eliminate potential errors arising from a lack of consideration of pertinent factors and capturing both linear and complex nonlinear interactions of the parameters, thus an accurate and detailed understanding of how the parameters influence bio-oil yields, this approach not only refines the pyrolysis process for coconut shell but surpasses conventional techniques in predictive capability and process control. This research advances prior studies by utilising hybrid models, PSO-ANFIS, and GA-ANFIS to improve prediction accuracy and process efficiency. The combination of these machine learning methods with experiments guarantees better modelling of parameter relationships, resulting in fewer experimental errors and greater optimization of bio-oil yields. The application

of Cocos nucifera serves as a biomass feedstock, broadening the scope of this work, especially in areas where the residues of coconut are in surplus. The synergy of the RSM and hybrid ANFIS models underlines the use of advanced computation techniques that might play a significant role in overcoming biomass conversion challenges, offering scalable solutions for both sustainable energy production and waste management.

2. Materials and Methods

2.1 Biomass source

The Cocos nucifera utilized for this research was sourced from Ota, a town in Ogun State, Nigeria, at a latitude of about 6.6985° N and a longitude of 3.2342° E. The sample was cleaned with distilled water to remove dirt and other impurities, after which it was dried in air for two days. The dried sample was then crushed into different sizes using a ball mill. The samples after drying were then weighed and sieved into the desired size distributions.

2.2 Biomass Characterization

Prior to experimentation, this study characterized the Cocos nucifera through its proximate and ultimate compositions as well as its structural composition and heating value to determine its energy potential for the pyrolysis process. Knowing these factors is critical to obtaining optimal pyrolysis conditions to maximize bio-oil yield while minimizing negative environmental impacts from the conversion process. This study analyses the biomass capability to serve as a renewable fuel for efficient pyrolysis by evaluating the key parameters of volatile matter, fixed carbon and ash contents, moisture contents, elemental composition, and the biomass higher and lower heating values.

The proximate analysis, such as moisture content, was determined by heating the biomass in a crucible furnace at 105°C according to ASTM D3173-02 (ASTM International, 2002), volatile matter at 900°C in an oxygen-free environment according to ASTM D3175-20 (ASTM International, 2020) and ash at 750°C using the standard test procedure outlined in ASTM D3174-02 (ASTM International, 2011). The Fixed Carbon (FC) denotes the solid combustible residue left behind after the volatile compounds are removed, while accounting for moisture (MC), volatile matter (VM), and ash content using Equation (1) (Akuwueke *et al*., 2024). A higher FC indicates a more energy-rich solid residue, which is important for pyrolysis yields and combustion potential. Also, ultimate analysis was used to determine the constituents of carbon, hydrogen, and nitrogen following the guidelines of ASTM D5373-16 (ASTM International, 2016). The sulphur content was obtained using ASTM D4239-11 (ASTM International, 2011) and the oxygen content was determined using Equation (2), while taking into account direct measurement of all other elements (carbon, hydrogen, nitrogen, sulfur, and ash) as proposed by (Onochie *et al*., 2023; Onokwai *at al*., 2022). Excessively high oxygen content lowered heating value and reduced stability of bio-oil. The structural composition includes lignin, which was obtained following the procedure outlined in ASTM D1106-21 (ASTM International, 2021), as well as cellulose and hemicellulose according to ASTM E1758. The higher heating value (HHV) was determined experimentally using a bomb calorimeter according to ASTM D5865-13 (ASTM International, 2013), while the lower heating value (LHV) was calculated from HHV as shown in Equation (3) by Oyebanji *et al.* (2023). This equation transforms the HHV into the LHV by factoring in the energy loss in vaporizing water formed when hydrogen burns. LHV is more useful in regard to practical purposes, such as biomass decomposition in the reactor. Gas chromatography-mass spectrometry (GC-MS) is used to identify compounds according to ASTM E1758-01(2020) (ASTM International, 2020), while Fourier-Transform Infrared Spectroscopy (FTIR) is used to determine the functional groups according to ASTM E1252-98 (ASTM International, 2013).

$$FC\ (wt.\%) = 100-(MC+VM+Ash\ content) \quad (1)$$

$$O\ (wt.\%) = 100 - (C + H + N + S + Ash) \quad (2)$$

$$LHV\ (MJ/kg) = HHV(MJ/kg) - (M \times H_2 \times \Delta H) \quad (3)$$

Where, FC is fixed carbon, MC moisture content, VM volatile matter, O, C, H, N, and S are oxygen, carbon, hydrogen, nitrogen, and sulphur contents, respectively; LHV is lower heating value; HHV is higher heating value; M is mass fraction of hydrogen in the biomass; H2 is Hydrogen – to - water conversion factor; and ΔH is latent heat of vaporisation of water

2.3 Modelling and Optimization Process

This study used RSM with CCD in experimental design as a statistical tool fit for optimization problems with multi-factor parameters when system behaviour could be described with a quadratic model. The matrix comprised operating parameters such as temperature (300-700°C), heating rate (6-30 °C/min), residence time (5-25 min), particle size (0.5-4.5 mm), and flow rate of nitrogen(10-50mL/min) with corresponding responses such as bio-oil, biochar, and non-condensable gases (NCG). Each parameter was considered at levels 1, -1, 0, α, and – α. The values – α and + α depend on a number of operating parameters in the parametric part of the design and were determined using Equation (4), where k was the number of operating parameters. The analysis came up with a mathematical expression linking the response variable and independent factors as explained in Equation (5).

$$\alpha = \pm[2\text{^}k]^{(1/4)} \quad (4)$$

$$y = f(x_1, x_2, x_3, \ldots\ldots\ldots\ldots x_n) \quad (5)$$

Where y is the response, f is the unknown response function, and x_1, x_2, x_3,……x_n are the independent factors, and n denotes their total number. These factors were assumed to be continuous and controllable within the experimental framework, ensuring minimal errors. Subsequently, the coefficients of a mathematical model were predicted using second-order or quadratic equations. This model was used for predicting, optimizing, identifying, and analysing the interaction influence of the independent parameters to determine their impact on the quality and quantity of bio-oil and biochar yields, as shown in Equation (6)

$$y = \beta_0 + \sum_{i=1}^{k} \beta_i x_i + \sum_{i=1}^{k} \beta_{ii} x_i^2 + \sum_{i=1}^{k} \sum_{j>1}^{k} \beta_{ij} x_i x_j + \epsilon \quad (6)$$

In Equation (5), x_i and x_j refer to the coded independent parameters, while y refers to the dependent variable or responses (bio-oil yield). The coefficients βo,β_i,β_{ii},and β_{ij} denote the constant term, linear effects, quadratic effects, and interaction effects, respectively. The term k indicates the number of independent factors, and ϵ_i accounts for random experimental errors.

The experiments were designed and analysed using the Design-Expert version 7.0.3, Stat-Ease, which automatically

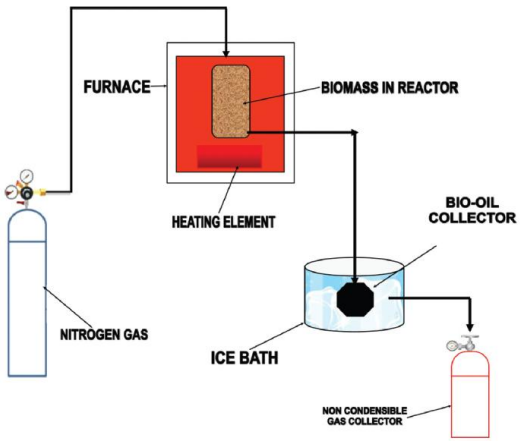

Fig 1. Experimental setup

solved the quadratic model to identify parameter interactions and evaluated statistical significance through P-values and the coefficient of determination (R^2). A high value of R^2 confirmed the model's reliability for the prediction of responses against the experimental conditions. In total, 50 experimental runs involving factorial, axial, and centre points for replication were carried out using CCD. The number of runs, N, was calculated using the formula for CCD given by Kumar *et al.* (2019) expressed in Equation (7).

$$N=2^k+2k+n_c \quad (7)$$

nc is the number of replicated experiments at the center; the 2k factorial design centered around the origin enables the derivation of a quadratic model with multiple independent factors. The design captured both linear and nonlinear interactions, allowing for a detailed assessment of each parameter's influence on bio-oil yield and process optimization.

2.4 Experimental Procedure

A pyrolysis plant comprising a fixed bed reactor, a PID temperature controller, a nitrogen gas cylinder, an ice bag condenser, a bio-oil collector, an NCG collector, and a 4kW electric heater is shown in Figure 1. The reactor system consisted of a tubular reactor made of 304 stainless steel in a vertical electric furnace that was fitted with a PID controller for good temperature control. A K-type thermocouple continuously measured the temperature and provided feedback to the controller, ensuring stable and precise temperature regulation. Biomass samples of Cocos nucifera (1.0–4.5 mm diameter, 100 g each) were fed into the reactor via a 10 L hopper. The reactor was preheated to operation temperatures of 300–700°C, having heating rates of 6–30°C/min and a residence time of 5–25 minutes. An inert nitrogen atmosphere is maintained with flow rates of 10–50 mL/min. Five runs for each experiment were conducted for consistency in the results obtained. The pyrolysis generated volatile gases, biochar, and bio-oil. The volatile gases passed through the condenser, which separated the bio-oil from water, while biochar was collected from the reactor. Yields were calculated by mass balance methods.

2.5. Predictive Modelling Using PSO-ANFIS and GA-ANFIS Based on Experimental Data

Hybrid machine learning models (PSO-ANFIS and GA-ANFIS) were utiised in this study to enhance the predictive capability and process optimization for bio-oil yield from *Cocos nucifera* pyrolysis due to their suitability in handling complex nonlinear relationships between process parameters and output yields (Cuevas *et al.*, 2024). These models were developed using real experimental data and benchmarked against traditional response surface methodology (RSM).

2.5.1 Data Collection and Preprocessing

The bio-oil yield was measured using input-output data from fifty (50) experimental pyrolysis runs whose process parameters had been varied systematically based on the experimental design matrix obtained using CCD. The corresponding output was bio-oil yield (wt.%), measured for each experiment. The dataset was divided into a training (70%) and a testing subset (30%) to develop and validate the predictive models. The input parameters (x) are temperature, heating rate, residence time, particle size, and nitrogen flow rate, while the output (y) is the bio-oil yield (wt.%). ANFIS, initialized with fuzzy rules and Gaussian membership functions (Titov, 2024), maps input-output relationships through the use of fuzzy logic and neural network learning. To enhance its sensitivity to parameters, optimization techniques PSO and GA were integrated for an improvement in predictive accuracy (Cuevas *et al.*, 2024).

2.5.2 ANFIS Structure and Initialization

The Adaptive Neuro-Fuzzy Inference System (ANFIS) model combines fuzzy logic reasoning with neural network learning. Initial fuzzy rules were generated from the training data, using Gaussian membership functions for each input variable. The model captured nonlinear interrelationships through a five-layer architecture that maps inputs to predicted outputs (bio-oil yields).

2.5.3 PSO-ANFIS Framework

ANFIS and PSO are adopted to optimise the bio-oil yield. The PSO was integrated with ANFIS to optimize the parameters (temperature, heating rate, residence time, particle size, and nitrogen flow rate) of the membership function with great efficiency. The ANFIS defines the fuzzy rules while a swarm of particles (potential solutions) is initialized, each encoding a set of ANFIS parameters. ANFIS predicts yields based on training data, and each particle calculates fitness, e.g., Mean Squared Error (MSE) and Coefficient of Determination (R^2) between predicted and actual values (Şener *et al.*, 2024). Particles iteratively update positions based on local and global best solutions until a stopping criterion, such as minimal error or maximum iterations, is met. This iterative feedback refines ANFIS parameters, enabling accurate and robust predictions as shown in Figure 2.

2.5.4 GA-ANFIS Framework

The GA-ANFIS framework (Figure 2) integrates ANFIS with GA to optimise bio-oil yield predictions. The GA-ANFIS model used a genetic algorithm to evolve the ANFIS parameters. Chromosomes represented fuzzy parameters and were evolved via selection, crossover, and mutation to iteratively refine a population of candidate solutions. The GA population encodes ANFIS parameters, including fuzzy rules and membership function shapes (Othman *et al.*, 2022). ANFIS predicts yields based on initial parameters, and the fitness of each chromosome was evaluated using the same MSE-based function. After several generations, the fittest chromosome provided the optimal ANFIS model configuration. This iterative process refines ANFIS parameters and enhances the capability of nonlinear relationship capture and predictive accuracy (Kumar & Bansal, 2023).

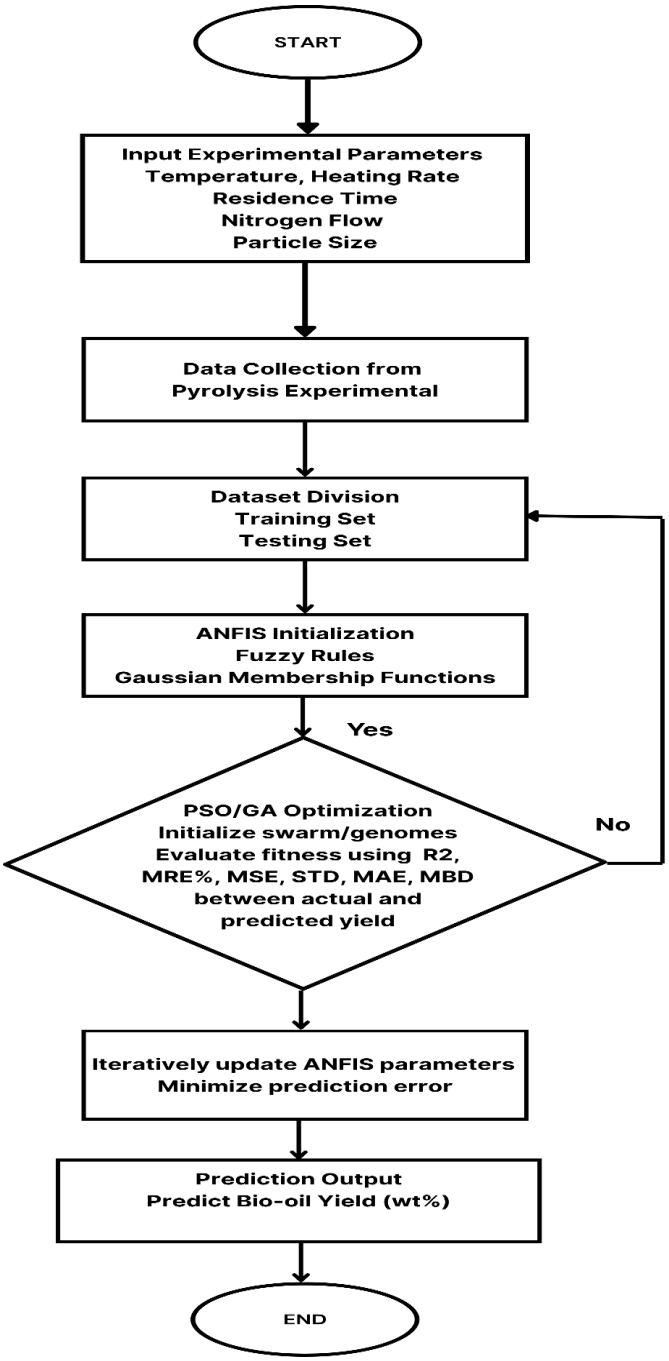

Fig 2. Computational Prediction of Bio-oil Yield Using PSO-ANFIS and GA-ANFIS Models

2.5.5 Model Evaluation Using Statistical Performance Metrics

The predicted bio-oil yield of the hybrid model was compared with the RSM model predictions, as the experimental values serve as a benchmark for the comparison. Although RSM efficiently models polynomial relationships, nonlinear, multi-modal interactions with biomass pyrolysis cannot be captured. This limitation is handled by the global optimization of PSO-ANFIS and GA-ANFIS, enhancing predictive accuracy and robustness (Abonyi *et al*., 2023; Onokwai *et al*., 2025). Various statistical metrics were computed using both training and testing datasets. These metrics collectively provide a comprehensive evaluation of the models in terms of accuracy, consistency, reliability, and bias, detailed as follows:

- *Coefficient of Determination (R^2)*

The coefficient of determination was employed to quantify the goodness of fit of the predicted values to the true experimental results, as shown in Equation 8 (Berggren, 2023). It represents the proportion of variance in the dependent variable that can be accounted for by the independent variables. The greater the value of R^2 and the closer to 1, the better the model fit to the data.

$$R^2 = 1 - \frac{\sum_{i=1}^{n}(y_i - \hat{y}_i)^2}{\sum_{i=1}^{n}(y_i - \bar{y})^2} \quad (8)$$

Where y_i is the experimental target values, $\hat{y}_i$ is the predicted value, $\bar{y}$ is the mean of experimental values, and n is the number of data points.

- *Mean Relative Error Percentage (MRE%)*

The Mean Relative Error Percentage (MRE%) is used to express the average relative deviation between predicted and experimental bio-oil yield as shown in Equation 9. The measure offered a normalized error, which provides a measure of the predictive capability of the model on a percentage scale (Özbay and Kokten, 2019).

$$\text{MRE\%} = \frac{1}{n}\sum_{i=1}^{n}\left|\frac{y_i - \hat{y}_i}{y_i}\right| \times 100 \quad (9)$$

- *Mean Squared Error (MSE)*

Mean Squared Error (MSE) is used to calculate the squared deviation of actual and predicted outputs as expressed in Equation 10. It measures of average squared error of prediction and is sensitive to large deviations (Djandja *et al*., 2023).

$$\text{MSE} = \frac{1}{n}\sum_{i=1}^{n}(y_i - \hat{y}_i)^2 \quad (10)$$

- *Root Mean Square Error (RMSE)*

The square root of MSE, known as the Root Mean Square Error (RMSE), has the same unit as the output variable (Equation 11). RMSE was utilised to interpret the predictive errors in the same units as the bio-oil yield (Mathur *et al*., 2022)

$$\text{RMSE} = \sqrt{\frac{1}{n}\sum_{i=1}^{n}(y_i - \hat{y}_i)^2} \quad (11)$$

- *Standard Deviation (STD)*

The Standard Deviation of Errors (STD) indicates the spread or dispersion of the errors of prediction from the mean (Equation 12). It provides information on the consistency and volatility of the performance of the model (Abbasi and Diwekar, 2014).

$$\text{STD} = \sqrt{\frac{1}{n}\sum_{i=1}^{n}\left((y_i - \hat{y}_i) - \frac{1}{n}\sum_{i=1}^{n}(y_i - \hat{y}_i)\right)^2} \quad (12)$$

- *Mean Absolute Error (MAE)*

The Mean Absolute Error (MAE) was used to calculate the average of the absolute difference between actual and predicted values, disregarding the direction of the error (Equation 13). This metric offers a simple-to-understand value for the size of the average error (Zhao *et al*., 2024).

$$\text{MAE} = \frac{1}{n}\sum_{i=1}^{n}|y_i - \hat{y}_i| \quad (13)$$

- *Mean Bias Deviation (MBD)*

The Mean Bias Deviation (MBD) was used to identify systematic overprediction or underprediction by the model (Equation 14). A positive or negative MBD indicates a tendency to overpredict or underpredict the target variable (Ahmed *et al*., 2024).

$$\text{MBD} = \frac{1}{n}\sum_{i=1}^{n}\left((y_i - \hat{y}_i)\right) \quad (14)$$

3. Results and Discussion

3.1. Characterization of Cocos nucifera

Table 1 outlines the characterization of *Cocos nucifera* biomass suitable for intermediate pyrolysis analysis. The proximate analysis comprises low moisture content (5.92 wt.%) to decrease energy loss and increase the yield of bio-oil, and high volatile matter (68.98 wt.%) and fixed carbon (23.20 wt.%) responsible for the production of bio-oil. The small ash content in the sample (1.90 wt.%) improves the biochar purity with a

Table 1
Biomass Characterization

Analysis	wt.%
Proximate analysis (wt.%)	
MC	5.92 + 0.001
VM	68.98 + 1.02
FC	23.20 + 0.13
Ash	1.90+ 0.01
Ultimate analysis (wt.%)	
C	49.93 + 0.12
H	6.92 + 0.04
N	0.91 + 0.01
O	42.04 + 0.13
S	0.20 + 0.001
Structural composition analysis (wt.%)	
Ce	33.25 + 0.04
He	28.31 + 0.10
Li	38.44 + 0.03
Heating value analysis (MJ/kg)	
HHV	22.96 + 0.01
LHV	20.17 + 0.02

reduction of reactor fouling. Ultimate analysis shows high carbon (49.93 wt.%) and moderate hydrogen (6.92 wt.%) content, indicating potential for energy-rich bio-oil. Oxygen content (42.04 wt.%) may affect stability and calorific value, while low sulphur (0.20 wt.%) reduces harmful emissions, supporting an environmentally friendly process (Abatyough *et al*., 2022). Pyrolysis was dependent on the structural composition of the biomass, cellulose, and hemicellulose, recorded at 33.25 wt.% and 28.31 wt.%, respectively, and decomposed at 300–500°C, which were the major contributors to bio-oil yield. Also, the degradation of lignin, 38.44 wt.%, at higher temperatures supports biochar yield. This shows that *Cocos nucifera* is a suitable pyrolysis feedstock. Moreover, the HHV, 22.96 MJ/kg, and the LHV, 20.17 MJ/kg, highlight potential energy sources (Ikpeseni *et al*., 2024; M. Kumar *et al*., 2019).

3.2 Experimental Design Matrix and Corresponding Response

Table 2 depicts the experimental design matrix and the corresponding responses (bio-oil, biochar, and NCGs) obtained from Fifty (50) experimental intermediate pyrolysis runs, while

Table 2
Experimental design matrix and the corresponding response

Run	Real level factors					Responses (wt.%)		
	A: Temperatures (°C)	B: Heating rates (°C/min)	C: Residence times (min)	D: Particle sizes (mm)	E: Nitrogen flow rates (mL/min)	Bio-oil	Biochar	NCG
1	500	18	10	2.5	30	52.17	21.28	26.91
2	500	18	15	2.5	30	49.51	22.31	28.18
3	500	18	5	2.5	30	49.73	24.41	25.86
4	700	30	25	0.5	50	44.21	21.08	34.71
5	300	6	5	4.5	10	41.11	47.21	11.68
6	500	18	15	2.5	30	49.33	22.35	28.32
7	500	12	15	2.5	30	48.64	22.47	28.89
8	700	6	5	4.5	10	45.93	42.91	11.16
9	700	30	5	4.5	10	46.21	33.11	20.68
10	300	30	25	4.5	10	38.12	36.61	25.27
11	300	30	25	0.5	10	45.56	30.63	23.81
12	400	18	15	2.5	30	48.43	23.91	27.66
13	500	18	15	2.5	30	49.58	22.38	28.04
14	300	6	5	0.5	10	46.83	45.18	7.99
15	300	6	25	0.5	10	43.21	40.09	16.7
16	500	18	15	2.5	20	50.76	21.94	27.3
17	700	30	25	4.5	50	35.21	23.15	41.64
18	700	6	25	0.5	50	43.21	24.76	32.03
19	300	30	5	0.5	10	47.53	37.81	14.66
20	300	30	25	4.5	50	32.19	31.76	36.05
21	500	18	15	2.5	30	49.47	22.36	28.17
22	300	30	5	4.5	10	45.67	43.67	10.66
23	700	30	5	4.5	50	44.27	25.84	29.89
24	300	6	25	4.5	10	36.16	44.36	19.48
25	500	18	15	1.5	30	51.43	23.12	25.45
26	700	30	5	0.5	50	41.1	22.09	36.81
27	300	6	5	4.5	50	40.21	46.22	13.57
28	500	18	15	2.5	30	49.43	22.4	28.17
29	500	24	15	3.5	40	48.21	21.94	29.85
30	700	30	5	0.5	10	47.78	25.23	26.99
31	700	6	25	4.5	10	39.31	34.13	26.56
32	500	18	15	2.5	30	49.56	22.34	28.1
33	300	6	5	0.5	50	46.41	41.16	12.43
34	500	18	15	2.5	10	49.2	24.54	26.26
35	700	30	25	0.5	10	46.24	23.55	30.21
36	300	6	25	0.5	50	40.25	32.61	27.14
37	600	18	15	2.5	30	48.18	22.81	29.01
38	700	6	25	0.5	10	45.91	26.58	27.51
39	500	18	15	2.5	30	49.53	22.41	28.06
40	700	6	5	0.5	50	47.16	27.61	25.23
41	500	18	15	2.5	50	49.01	23.71	27.28
42	700	6	5	0.5	10	47.53	35.12	17.35
43	300	30	5	0.5	50	47.36	37.81	14.83
44	300	30	5	4.5	50	42.48	38.12	19.4
45	300	6	25	4.5	50	30.01	39.29	30.7
46	700	6	25	4.5	50	33.54	28.13	38.33
47	700	6	20	4.5	50	34.27	29.54	36.19
48	700	30	25	4.5	10	37.12	24.01	38.87
49	500	18	15	2.5	30	49.63	22.38	27.99
50	300	30	25	0.5	50	44.21	24.04	31.75

Table 3
Correlation between real and coded levels of operating parameters of the intermediate pyrolysis process

	Level				
Operating parameter	**Axial (-α)**	**Low**	**Center**	**High**	**Axial (+α)**
	-2	-1	0	1	2
Temperature (°C)	300	400	500	600	700
Heating rate (°C/min)	6	12	18	24	30
Residence time (min)	5	10	15	20	25
Particle size (mm)	0.5	1.5	2.5	3.5	4.5
Nitrogen flow rate (mL/min)	10	20	30	40	50

Table 3 shows the correlation between real and coded values. The factors influenced the pyrolysis products, with temperature being the most influential. The highest bio-oil yield, for Run 1 at a temperature of 500°C, was 52.17 wt.%, since this temperature was adequate to provide the necessary thermal energy for volatile compound formation with reduced secondary cracking. At lower temperatures, such as 300°C, in Run 20, the yield decreased to 32.19 wt.% owing to incomplete pyrolysis and restricted volatile formation (Afrah *et al*., 2024).

At high temperatures, 700°C, secondary cracking of bio-oil vapours into NCGs occurs, which reduces bio-oil yields, as seen in Run 17 (35.21 wt.%). In contrast, low temperatures favour biochar production due to limited devolatilization, in Run 5 at 300°C, yielding 47.21 wt.%. As temperature increases, volatile matter evolution rises, lowering biochar yields while boosting NCG production, exemplified in Run 17, where NCG yield reached 41.64 wt.%. The heating rate significantly impacts pyrolysis outcomes. Moderate rates (18°C/min) optimise bio-oil yields (50 wt.%, Runs 1, 16, 32) by balancing decomposition and minimizing secondary reactions. High rates (30°C/min) enhance thermal cracking, increasing NCG yields (41.64 wt.%, Run 17) at the expense of bio-oil and biochar. Conversely, low rates (6°C/min) favour biochar yields (47.21 wt.%, Run 5) due to slower volatilization. Residence time affects primary pyrolysis and secondary reactions. Shorter residence times, such as 5 minutes, favour higher bio-oil yields, 46.21 wt.% for Run 9, by reducing secondary decomposition. Longer residence times, such as 25 minutes, increase NCG yields, 41.64 wt.% for Run 17, due to increased thermal cracking, repolymerisation, and recondensation, which decrease bio-oil and biochar yields. Particle size affects heat transfer and product distribution (Hasan *et al*., 2023). Smaller sizes (<0.5 mm) improve bio-oil and NCG yields, as seen in Run 30 (36.81 wt.% NCG at 700°C), while larger sizes (4.5 mm) limit heat penetration, increasing biochar yields (47.21 wt.% in Run 5, 44.36 wt.% in Run 24). The nitrogen flow rate maintains the reaction environment. A higher flow rate (50 mL/min) reduces the concentrations of reactive vapour and secondary cracking, hence improving the bio-oil yield to 46.41 wt.% at 300°C for Run 33. Lower flow rates, such as 10 mL/min, promote secondary reactions and increase NCG yield to 36.05 wt.% for Run 20.

3.3 Statistical Model Development for bio-oil yield via intermediate pyrolysis process

Table 4 and Equation (4) present the effects of pyrolysis parameters, such as temperature (A), heating rate (B), residence time (C), particle size (D), and nitrogen flow rate (E), on bio-oil

Table 4
ANOVA for Reduced Quadratic model for Bio-oil Yields (BO)

Source	**Sum of Squares**	**df**	**Mean Square**	**F-value**	**p-value**	**Remark**
Model	1396.52	10	139.40	76.76	< 0.0001	significant
A-Temperatures	66.11	1	66.11	36.40	< 0.0001	significant
B-Heating rates	9.92	1	9.92	5.46	0.0246	significant
C-Residence times	230.40	1	230.40	126.86	< 0.0001	significant
D-Particle sizes	287.56	1	287.56	158.33	< 0.0001	significant
E-Nitrogen flow rates	10.60	1	10.60	5.84	0.0205	significant
AB	13.31	1	13.31	7.33	0.0100	significant
AD	9.66	1	9.66	5.34	0.0281	significant
CD	75.82	1	75.82	41.75	< 0.0001	significant
CE	6.04	1	6.04	3.32	0.0759	Not significant
A^2	562.25	1	562.25	309.59	< 0.0001	significant
Residual	5.67	39	1.82			
Lack of Fit	8.61	32	3.88	2.69	0.1090	Not significant
Pure Error	0.0624	7	0.0089			
Cor Total	1405.19	49				

R^2 =98.16 wt.%; Adjusted R^2 =93.92 wt.%; Predicted R^2 = 90.89 wt.%; CV = 3.01 wt.%; Adeq Precision = 33.5481

yield. The complicated relationships were well described by the quadratic models, reflected in the statistical parameters R^2, Adeq Precision, values of lack-of-fit, and CV. The model for bio-oil yield was highly significant with an F-value of 76.76 and $p < 0.0001$. Obtained Adeq Precision of 33.55, showing a high signal-to-noise ratio, and the non-significant lack-of-fit ($p = 0.1090$), confirming the reliability of the model. Low CV (3.01 wt.%) and high R^2 (98.16 wt.%) validated the model, and adjusted R^2 (93.92 wt.%) and predicted R^2 (90.89 wt.%) confirmed predictive accuracy. With an F-value of 36.40 and $p < 0.0001$, the temperature had a significant influence on bio-oil yield. Also, other variables such as residence time and particle size show good influence; longer residence time favours volatile matter release, and smaller particle size enhances heat transfer. Interaction effects, such as AB (temperature and heating rate, $p = 0.0100$) and CD (residence time and particle size, $p < 0.0001$), synergistically enhance bio-oil recovery. The quadratic temperature term (F-value = 309.59) highlights a nonlinear relationship, with bio-oil yield increasing before leveling off or declining at higher temperatures (Ikpeseni *et al.*, 2024). The statistical parameters confirm the reliability and precision of the model, such as Adeq Precision (33.55), lack-of-fit values, and CV. High Adeq Precision and non-significant lack-of-fit prove the accuracy of the model for predictions, while low CV establishes the suitability for optimization of pyrolysis. With high R^2 values, the model effectively enhances yields through synergistic effects with minimum antagonist influences for specific applications.

$$Y_{BO} = 7.3079 + 0.1842A + 0.1811B - 0.00615C - 0.9068D - 0.0362E - 0.0003AB + 0.0012AD - 0.0786CD - 0.00222CE - 0.000179A^2 \quad (15)$$

Where; Y_{BO} is bio-oil (in wt.%) yield, A, B, C, D, and E, represents temperature (°C), heating rate (°C/min), residence time (min), particle sizes (mm), and nitrogen flow rate (mL/min), respectively.

3.4 *Influence of Individual Parameters on the Bio-Oil Yield*

Figure 4a shows that the influence of temperature on bio-oil yield increases with temperature, peaking at 45 wt.% around 500°C due to the decomposition of hemicellulose and cellulose and secondary degradation of biochar. However, above 500°C, yields begin to drop, which can be attributed to secondary cracking, where the liquid intermediates at higher temperatures further crack into lighter NCGs. Figure 3b shows the influence of heating rates, where bio-oil yields increase with higher rates, reaching 48 wt.% at 30°C/min. Faster heating enhances devolatilization while reducing residence time for secondary cracking. In contrast, lower heating rates (6°C/min) yield about 30 wt.% bio-oil but favour char production, demonstrating the importance of heating rates in pyrolysis (Jalalifar, 2020). Figure 3c depicts the effect of residence time. At shorter times (5 minutes), bio-oil yield is highest at 45 wt.%, while longer times (25 minutes) reduce yields to 30 wt.% due to increased secondary cracking. Short residence times thus favour bio-oil production. Figure 3d highlights the impact of particle size, with smaller particles (0.5 mm) yielding up to 51 wt.% bio-oil due to better heat transfer and mass diffusion. Larger particles (4.5 mm) produce less bio-oil (42.1 wt.%) and more char due to slower heat penetration and incomplete pyrolysis. Figure 3e explores the effects of nitrogen flow rate. Bio-oil yield increases with flow rates up to 30 mL/min, reaching 45 wt.% due to improved volatile removal and reduced secondary cracking (Laougé *et al.*, 2020). Beyond 30 mL/min, yields decline to 40 wt.% at 50 mL/min, likely due to vapour dilution and reduced condensation efficiency.

3.5 *Influence of the Two Most Significant Factors on Bio-oil Yield*

Figures 5(a-b) to 6(a-b) present a 3D response surface and 2D contour plots on the interrelationship among key parameters involved in the bio-oil yield. Figure 4a illustrates the interaction of temperature and heating rates on the yield of bio-oil, while Figure 4b presents its 2D contour plot for optimization. The maximum bio-oil yield of 51 wt.% was observed at 500°C and

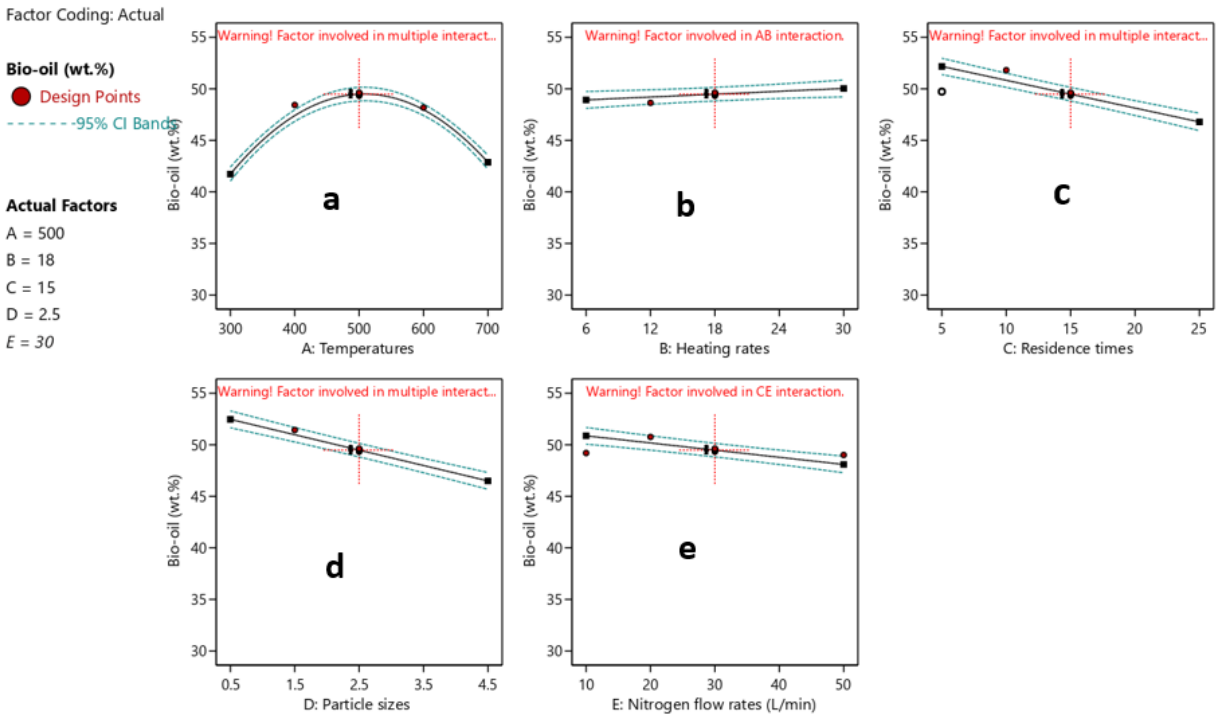

Fig 4. Influence of (a) temperature, (b) heating rate, (c) residence time, (d) particle sizes, (e) nitrogen flow rate on the bio-oil yield

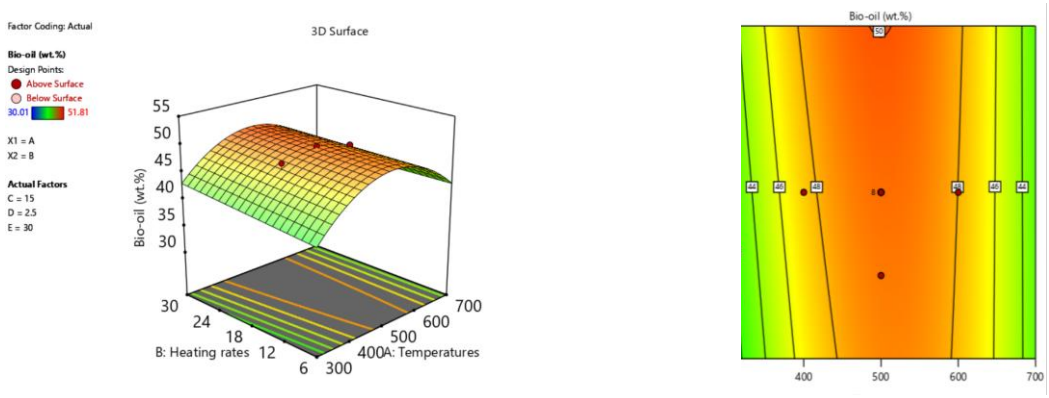

a b

Fig 5 (a) 3D surface plot of bio-oil (wt.%) against temperature (°C) and heating rates (°C/min(b) 2D contour plot of bio-oil (wt.%) against temperature (°C) and heating rates (°C/min).

30°C/min. These are conditions that maximize the thermal decomposition of biomass components into volatiles. These conditions, combined with residence time, particle size, and nitrogen flow rate of 15 minutes, 2.5 mm, and 30 mL/min, respectively, minimize external influences on bio-oil production. Above 500°C, bio-oil yield decreases because of the secondary cracking of volatiles into smaller gaseous molecules. But below 500°C, fewer volatiles are produced due to the low activation energy to have complete decomposition. The heating rates also have a strong impact on bio-oil production. At 30°C/min, there is an optimum balance between primary pyrolysis and a minimal amount of secondary reactions, leading to the highest yield of 51.2 wt.%. Above this rate, increased secondary cracking reduces the yields, while below this rate, longer thermal exposure causes excessive charring and volatile loss. The results emphasize the need to balance temperature and heating rates for maximum bio-oil yield. Optimal conditions (500°C, 30°C/min) provide efficient energy input and controlled reaction dynamics, minimizing secondary reactions while maximizing biomass conversion into bio-oil. This highlights the importance of precise parameter optimization for efficient and sustainable pyrolysis processes.

Figure 6 shows the relationship between temperature vs. particle size for the optimization of bio-oil yield in both 3D and 2D plots. Indeed, the maximum bio-oil yield of 49.5 wt.% was obtained at 500°C with a particle size of 0.5 mm, which will allow the effective thermal decomposition of biomass into volatile products with a reduced amount of secondary reactions. Other parameters, like the heating rate of 18°C/min, residence time of 15 minutes, and nitrogen flow of 30 mL/min, were kept constant to isolate these effects. Temperature is another critical parameter that influences the production of bio-oil. At 500°C, enough energy depolymerizes cellulose, hemicellulose, and lignin into volatiles without favouring secondary reactions. Above 500°C, the yields declined owing to increased secondary cracking, while below 500°C, incomplete decomposition is limiting volatile production. For instance, lower yields at 400°C are a result of restricted volatilization. Particle size significantly influences bio-oil yield. A size of 0.5 mm ensures rapid and uniform heat transfer for efficient decomposition, while larger sizes (>1.5 mm) limit heat penetration, reducing yields. Smaller sizes (<0.5 mm) cause excessive charring, also lowering yields. The optimal combination of 500°C and 0.5 mm particle size highlights the importance of precise parameter optimization for improving pyrolysis efficiency and maximizing bio-oil yield (Di Lauro *et al*., 2024).

Figure 7 illustrates the interaction between residence time and particle size in influencing bio-oil yields during pyrolysis. A 3D surface plot (Figure 6a) and a 2D contour plot (Figure 6b) highlight that the highest bio-oil yield (50.5 wt.%) was achieved at a residence time of 15 minutes with a particle size of 0.5 mm. The specified conditions led to efficient thermal decomposition through which volatiles condensed into bio-oil while secondary reactions remained minimal. Constant control conditions consisting of a temperature (500°C), heating rates (18°C/min), and nitrogen flow rates (30 mL/min), provided a stable pyrolysis

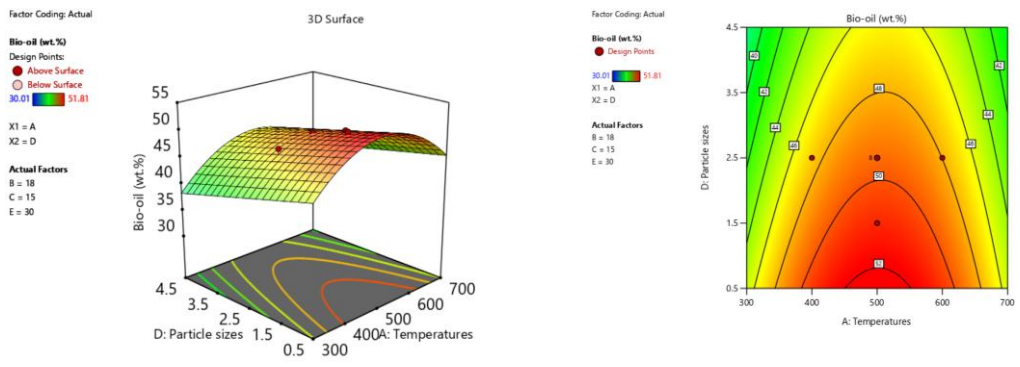

a b

Fig 6 (a) 3D surface plot of bio-oil (wt.%) against temperature (°C) and particle sizes (mm) (b) 2D contour plot of bio-oil (wt.%) against temperature (°C) and particle sizes (mm).

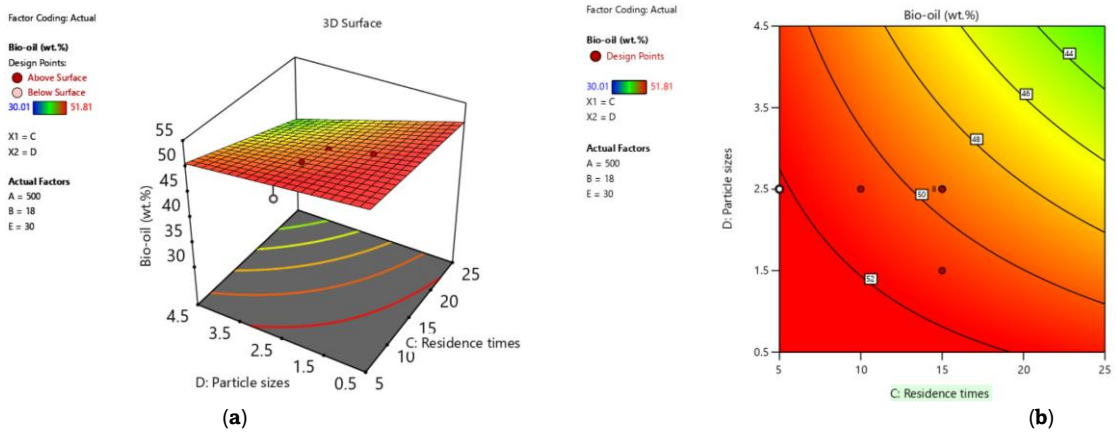

Fig 7 (a) 3D surface plot of bio-oil (wt.%) against residence time (min) and particle sizes (mm) (b) 2D contour plot of bio-oil (wt.%) against residence time (min) and particle sizes (mm).

environment to investigate the influence of residence time and particle size. Bio-oil production showed a strong dependency on residence time. The biomass stayed within the reactor. During the 15-minute thermal exposure, the biomass particles received adequate thermal energy, leading to complete vapourisation without generating excessive secondary reactions. Time prolongation caused secondary chemical reactions that decreased product yields, while shorter times resulted in incomplete volatile decomposition. Bio-oil production exhibited a strong dependence on particle sizes. A particle size of 0.5 mm ensured uniform heat transfer for efficient decomposition, while larger particles (>1.5 mm) suffered from poor heat penetration, and smaller particles (<0.5 mm) caused excess charring, both reducing yields. The interplay between residence time and particle size was crucial for maximizing bio-oil production. The optimal combination of 15 minutes and 0.5 mm enabled efficient decomposition with minimal secondary reactions, yielding 50.5 wt.% of bio-oil. These findings underscore the importance of parameter optimization for achieving efficient and sustainable pyrolysis under controlled conditions.

3.6 Accuracy and Reliability of RSM model using Residual, Leverage, Cook's distance, and Fitted Value DFFITS

Figure 8a shows the scatterplot of actual vs. predicted bio-oil yields using RSM, demonstrating a high correlation between experimental results and model predictions. Data points are tightly clustered around the diagonal line, indicating strong model performance with minor deviations due to experimental variability or model constraints. Variations in scatter suggest that refining model parameters could improve accuracy, as supported by (Chantarangsi *et al*., 2015; Jalalinejad *et al*., 2024). Figure 7b presents the normal probability plot of residuals for bio-oil, used to assess the adequacy of the predictive model. Residuals align closely with the diagonal line, confirming their approximate normal distribution, a key regression assumption (Kozak & Piepho, 2018; Nawaz *et al*., 2024). The slight non-normality detected at the extremes does not affect the model's reliability. The external studentized residual plot reveals that most points follow the diagonal line with no data points exceeding the ±2 or ±3 typical outlier thresholds. The results indicate there are no significant influencing data points affecting the regression coefficient values. The model demonstrates robustness based on the combined analysis of residuals and external studentized residuals. The model exhibits predictive power because residuals show normal distribution, along with no detectable outliers. Furthermore, the model exhibits strong predictive capabilities for bio-oil yield assessment through comprehensive statistical analysis that reveals minor errors related to nonlinear effects. The model demonstrates robustness in predicting bio-oil yield through its tested results,

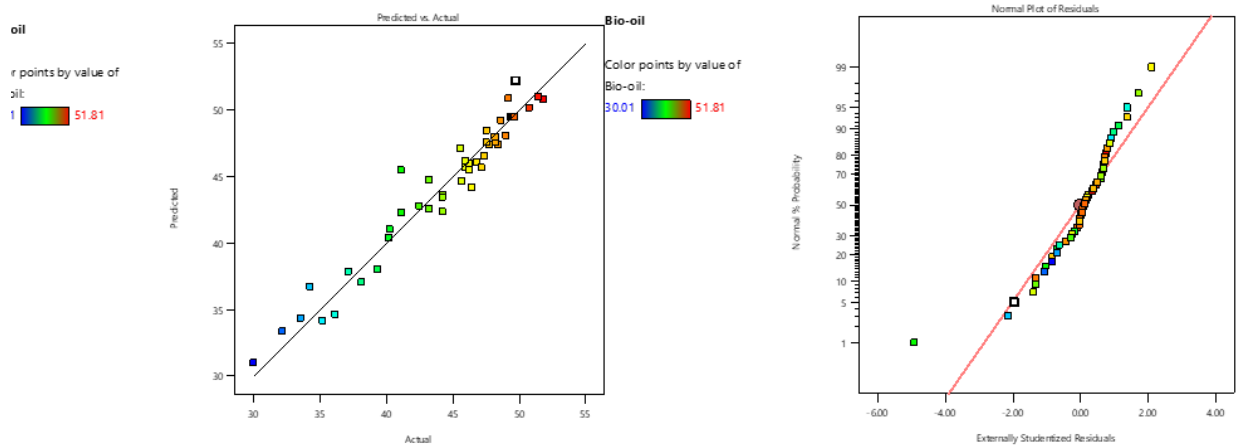

Fig 8 (a) Actual vs Predicted (b) Normal probability plot of residuals

but research continues to develop methods for improving accuracy by incorporating nonlinear effects.

3.7 Comparison Analysis between Experimental, RSM, and ANFIS Models Predicted Bio-oil Yields

The actual and predicted bio-oil yields from intermediate *Cocos nucifera* pyrolysis using GA-ANFIS, PSO-ANFIS, and RSM methods are compared in Table 5. The analysis evaluates model performance across various experimental conditions, including temperature, heating rate, residence time, particle size, and nitrogen flow rate. The actual bio-oil yield stands as the benchmark for evaluating the accuracy of prediction models. The prediction technique PSO-ANFIS possesses the most accurate numerical outcomes compared to experimental values, demonstrating excellent prediction accuracy. The predicted bio-oil yield in Run 1 from PSO-ANFIS was 51.59 wt.% and proved more accurate than both RSM's prediction of 50.83 wt.% and GA-ANFIS's result of 52.17 wt.%. The bio-oil yield prediction in Run 16 reaches 51.01 wt.% using PSO ANFIS analysis while maintaining superior accuracy compared to other prediction models. GA-ANFIS exhibits strong prediction abilities, but its predictive deviations remain slightly higher than

Table 5
Comparison of Actual Bio-oil Yields with RSM, PSO-ANFIS, and GA-ANFIS Predictions

Std	Run	Factor 1 A: Temperatures oC	Factor 2 B: Heating rates oC/min	Factor 3 C: Residence times minutes	Factor 4 D: Particle sizes Mm	Factor 5 E: Nitrogen flow rates mL/min	Actual Bio-oil wt.%	RSM Bio-oil wt.%	GA-ANFIS Bio-oil wt.%	PSO-ANFIS Bio-oil wt.%
36	1	500	18	10	2.5	30	52.17	50.83	52.17	51.59
48	2	500	18	15	2.5	30	49.51	49.48	49.59	49.68
35	3	500	18	5	2.5	30	49.73	52.18	49.81	49.89
16	4	700	30	25	0.5	50	44.21	42.34	44.20	44.30
17	5	300	6	5	4.5	10	41.11	42.28	41.19	41.31
47	6	500	18	15	2.5	30	49.33	49.48	49.40	49.49
37	7	500	12	15	2.5	30	48.64	49.21	48.71	48.82
18	8	700	6	5	4.5	10	45.93	45.67	46.01	46.11
22	9	700	30	5	4.5	10	46.21	45.48	46.19	46.37
23	10	300	30	25	4.5	10	38.12	37.04	38.18	38.30
7	11	300	30	25	0.5	10	45.56	47.10	45.68	45.81
34	12	400	18	15	2.5	30	48.43	47.40	48.51	48.57
43	13	500	18	15	2.5	30	49.58	49.48	49.61	49.70
1	14	300	6	5	0.5	10	46.83	46.05	46.90	47.11
3	15	300	6	25	0.5	10	43.21	44.70	43.31	43.41
39	16	500	18	15	2.5	20	50.76	50.18	50.87	51.01
32	17	700	30	25	4.5	50	35.21	34.17	35.40	35.48
12	18	700	6	25	0.5	50	43.21	42.53	43.31	43.41
5	19	300	30	5	0.5	10	47.53	48.46	47.71	47.81
31	20	300	30	25	4.5	50	32.19	33.37	32.42	32.49
44	21	500	18	15	2.5	30	49.47	49.48	49.49	49.61
21	22	300	30	5	4.5	10	45.67	44.68	45.79	45.91
30	23	700	30	5	4.5	50	44.27	43.59	44.38	44.52
19	24	300	6	25	4.5	10	36.16	34.63	36.30	36.40
42	25	500	18	15	1.5	30	51.43	50.98	51.61	51.70
14	26	700	30	5	0.5	50	41.1	45.47	41.20	41.30
25	27	300	6	5	4.5	50	40.21	40.39	40.39	40.48
41	28	500	18	15	2.5	30	49.43	49.48	49.49	49.61
38	29	500	24	15	3.5	40	48.21	47.57	48.31	48.42
6	30	700	30	5	0.5	10	47.78	47.36	47.87	48.01
20	31	700	6	25	4.5	10	39.31	38.03	39.50	39.61
46	32	500	18	15	2.5	30	49.56	49.48	49.58	49.72
9	33	300	6	5	0.5	50	46.41	44.16	46.50	46.60
50	34	500	18	15	2.5	10	49.2	50.87	49.31	49.40
8	35	700	30	25	0.5	10	46.24	46.01	46.40	46.51
11	36	300	6	25	0.5	50	40.25	41.03	40.41	40.49
33	37	600	18	15	2.5	30	48.18	47.97	48.31	48.37
4	38	700	6	25	0.5	10	45.91	46.19	46.03	46.11
49	39	500	18	15	2.5	30	49.53	49.48	49.61	49.71
10	40	700	6	5	0.5	50	47.16	45.65	47.19	47.41
40	41	500	18	15	2.5	50	49.01	48.09	49.18	49.31
2	42	700	6	5	0.5	10	47.53	47.54	47.69	47.78
13	43	300	30	5	0.5	50	47.36	46.57	47.49	47.57
29	44	300	30	5	4.5	50	42.48	42.79	42.61	42.70
27	45	300	6	25	4.5	50	30.01	30.97	30.11	30.21
28	46	700	6	25	4.5	50	33.54	34.36	33.71	33.78
26	47	700	6	20	4.5	50	34.27	36.71	34.40	34.50
24	48	700	30	25	4.5	10	37.12	37.84	37.31	37.41
45	49	500	18	15	2.5	30	49.63	49.48	49.61	49.70
15	50	300	30	25	0.5	50	44.21	43.44	44.30	44.41

Table 6
Performance Metrics of Different Statistical Parameters for Bio-oil Prediction Models

Model	Phase	R^2	MRE%	MSE	RMSE	STD	MAE	MBD
PSO-ANFIS	Train	0.998	0.641	0.093	0.305	0.367	0.202	0.058
	Test	0.994	0.981	0.202	0.449	0.492	0.319	0.127
GA-ANFIS	Train	0.996	0.821	0.146	0.382	0.414	0.297	0.099
	Test	0.991	1.152	0.304	0.551	0.591	0.418	0.185
RSM	Train	0.981	2.451	1.372	1.171	1.226	0.875	0.531
	Test	0.974	3.024	1.893	1.376	1.471	1.097	0.734
Experimental	Train	1	0	0	0	0	0	0
	Test	1	0	0	0	0	0	0

Table 7
ANOVA: Two-Factor With Replication

Source of Variation	SS	df	MS	F	P-value	F crit
Sample	0.189254	1	0.189254	1.787341	0.218018	5.317655
Columns	0.03318	1	0.03318	0.313357	0.590952	5.317655
Interaction	0.00118	1	0.00118	0.011145	0.918523	5.317655
Within	0.847087	8	0.105886			
Total	1.070701	11				

PSO-ANFIS. The actual bio-oil yield of 49.33 wt.% in Run 6 closely aligns with GA-ANFIS predictions of 49.40 wt.% and PSO-ANFIS predictions of 49.49 wt.%. The consistent accuracy of PSO-ANFIS surpasses GA-ANFIS across multiple runs. RSM, as a statistical approach, demonstrates the greatest deviation from actual values among the other models. The RSM model predicts a bio-oil yield of 34.17 wt.% in Run 17 against the actual value of 35.21 wt.%, while PSO-ANFIS and GA-ANFIS demonstrated smaller deviations. RSM's prediction for bio-oil yield at 38.03 wt.% in Run 31 further shows evidence of its reduced predictive capability when compared to the actual value of 39.31 wt.%. Hence, RSM demonstrates a limited ability to detect non-linear relationships between operating parameter interactions and bio-oil yield(Mbah *et al*., 2024).

Table 6 presents comprehensive performance metrics of bio-oil prediction models consisting of PSO-ANFIS, GA-ANFIS, and RSM. This study evaluated the performance of bio-oil prediction models using coefficient of determination (R^2), mean relative error (MRE%), mean squared error (MSE), root mean squared error (RMSE), standard deviation (STD), mean absolute error (MAE), and mean bias deviation (MBD), that were evaluated on both training and testing phases. PSO- ANFIS proves to be the most accurate among the prediction models with a training R^2 of 0.998 and testing R^2 of 0.994, establishing strong relationships between predicted and actual bio-oil yields. During both the training and testing phases, the PSO-ANSIS maintained the minimum errors, with a training and testing MRE% of 0.641% and 0.981%, respectively. Likewise, the MSE and RMSE values demonstrate superior performance to other models, thus affirming the efficiency of the reduction of prediction error. The prediction bias from the PSO-ANFIS model appears minimal due to the low MBD values. The training and testing R^2 from GA-ANFIS were 0.996 and 0.991, respectively. PSO-ANFIS demonstrates superior error metrics than GA-ANFIS due to its training MRE% of 0.821% and testing MRE% of 1.152%. The GA-ANFIS model demonstrates strong prediction abilities, based on training RMSE of 0.382 and testing RMSE of 0.551, though its predictions show slightly more deviation from actual values than PSO ANFIS. Among all the models, RSM shows the lowest performance. The predictive power of RSM stands below PSO-ANFIS and GA-ANFIS as it possesses a training R^2 of 0.981 and a testing R^2 of 0.974. The model demonstrates significant error rates, such that it exhibits a training MRE% of 2.451% and a testing MRE% of 3.024%. The prediction models show higher deviation from bio-oil values due to their training RMSE of 1.171 and testing RMSE of 1.376. RSM demonstrates higher predictive bias than PSO-ANFIS and PSO-ANFIS due to its high MBD metric values. The experimental results function as a benchmark that shows flawless results across every metric. This affirms the reliability of the bio-oil yields and aids in model validation.

This study analyses hybrid models designed to optimize biomass pyrolysis, illustrating their wider application across different feedstocks. The novelty of this study is grounded on the superior prediction accuracy of the PSO-ANFIS model (R^2 = 0.998, RMSE = 0.305) during training, which is more robust than RSM and traditional machine learning methods by a wide margin, while GA-ANFIS was also accurate, but with slightly lower precision. With these models, operators can estimate the quantity of bio-oil yield, optimize critical parameters like temperature, heating rates, residence time, nitrogen flow rate, and particle size, and minimize the number of experimental trials needed. The use of these hybrid models improves the prediction and optimization of bio-oil yield, which enhances the process uncertainties and efficiency improvements in biomass conversion. These features allow for dynamic changes to be made during the process, improving bio-oil quality and process efficiency. Also, the bio-oil produced under those conditions has lower oxygen content and higher energy density, making it more applicable for industrial usage. The study reinforces the

Table 8
Numerical Model Improvement Over RSM (Test Phase)

Metric	PSO-ANFIS vs RSM	GA-ANFIS vs RSM
R^2	↑ by 1.76%	↑ by 2.06%
MRE (%)	↑ by 1.86%	↑ by 2.03%
MSE	↑ by 1.57%	↑ by 1.68%
RMSE	↑ by 0.81%	↑ by 0.91%
MAE	↑ by 0.65%	↑ by 0.76%
MBD	↑ by 0.53%	↑ by 0.60%

claim of the economic and environmental efficiency of computational modelling in reducing waste and optimizing resource utilization for large-scale bio-oil production.

Results obtained from the ANOVA (Table 7) show that no significant differences exist statistically amongst the models tested. The effect sample with an F-value of 1.7873 and a P-value of 0.2180 does not exceed the critical value of 5.3177, implying that the variation across samples is not significant. Likewise, the column effect with an F value of 0.3134 and a P value of 0.5909 is also non-significant, meaning that differences between columns do not significantly alter the outcome metrics. In addition, the interaction effect between the factors with an F-value of 0.0111 and a P-value of 0.9185 is insignificant, further confirming that these factors do not affect the results. These findings suggest that any changes observed in the performance metrics computed for RSM with GA-ANFIS and PSO-ANFIS are random variations, rather than any systematic deviations. Hence, while some models may exhibit marginally lower error results, they do not pass the significance threshold as verified by the ANOVA test

The hybrid models GA-ANFIS and PSO-ANFIS showed clear improvement when compared to the traditional model (RSM) in the test phase (Table 8). The R^2 value, reflecting the fit between predicted and actual bio-oil yields, increased by 1.76% for GA-ANFIS and 2.06% for PSO-ANFIS. Although modest, these gains are significant in modelling complex, nonlinear systems like biomass pyrolysis. The hybrids also demonstrated lower mean relative error (MRE) than the traditional model, with GA-ANFIS reducing it by 1.86% and PSO-ANFIS by 2.03%, proving their accuracy and consistency. Improvements, further extended to absolute error metrics, where MSE was reduced by 1.57 and 1.68 units, and RMSE by 0.81 and 0.91 units for GA-ANFIS and PSO-ANFIS, respectively. The MAE decreased by 0.65 and 0.76, while MBD went down by 0.53 and 0.60, from both models, confirming the hybrid models' ability to reduce systematic prediction errors. Among the models, PSO-ANFIS consistently outperformed others. The results of this analysis underscored the superior predictive accuracy, robustness, reliability, and generalization of hybrid intelligent models, especially PSO-ANFIS, when it comes to optimizing bio-oil yield under complex pyrolysis conditions.

3.7 Optimum Conditions of Operating Parameters

Figure 9 presents optimization plots for bio-oil yield during the pyrolysis of *Cocos nucifera* biomass, illustrating the influence of key parameters: temperature, heating rate, residence time, particle size, and nitrogen flow rate. The results indicate an extensive improvement in predicting and optimizing bio-oil yield. The optimal bio-oil yield (52.2 wt.%) was attained at a temperature of 510.2°C, heating rates of 10.5°C/min, residence time of 5.2 min, a particle size of 0.3, and nitrogen flow rate of 17.3 mL/min. Beyond 510°C, excessive cracking reduces bio-oil yield and increases NCG production. Continuous increase in heating rates ensures uniform thermal degradation, avoiding the reduced yields associated with both higher and lower rates. The optimal residence time range is between 5 and 10 minutes helps maximize bio-oil yield and extend times in the

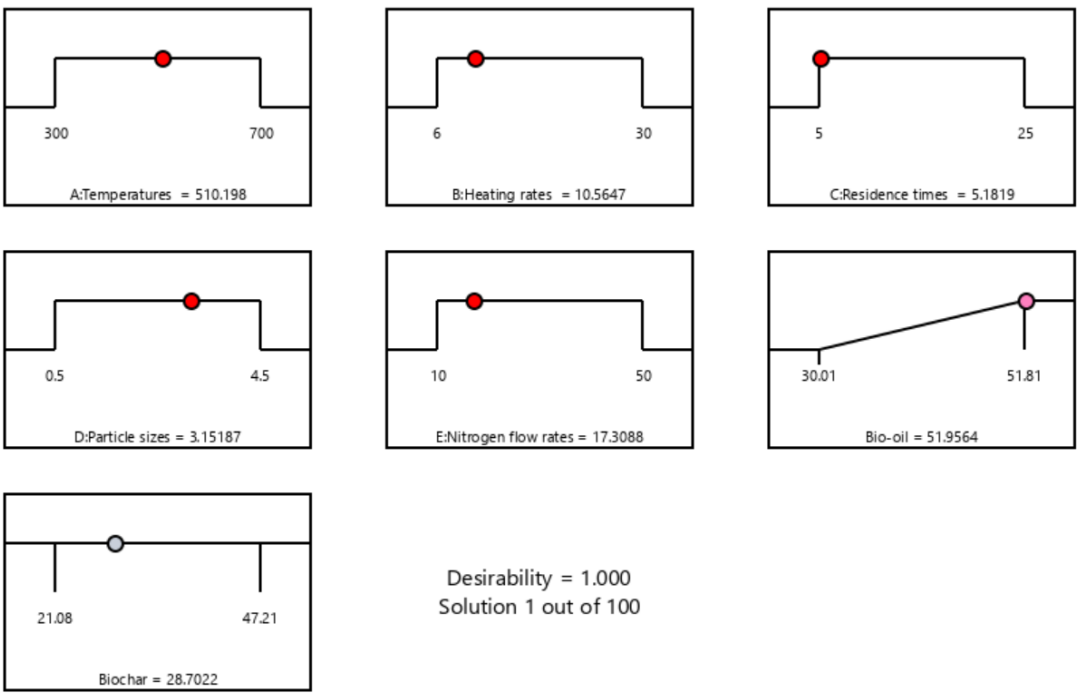

Fig 9. Optimization plot for bio-oil

conversion of primary reactants to NCG. Particle sizes between 0.3 – 0.5 mm produce efficient heat transfer along with uniform decomposition reactions, and the nitrogen flow rates between 10 to 20 mL/min support an inert environment that enhances bio-oil yield through minimized secondary cracking processes. Bio-oil obtained during these specific operating conditions is well-suited for renewable fuel production along with biochemical feedstock applications due to its stable performance and high energy content, alongside minimal oxygen compounds (Wulandari *et al*., 2020). Figure 9 presents an optimization approach that systematically integrates these parameters, that minimises empirical methods, time, costs, and resource usage. This research differs from traditional single-product approaches to achieve optimal bio-oil yields for diverse applications. The utilisation of particle size and nitrogen flow rate as critical factors enhances the novelty and practicality of biomass pyrolysis processes by addressing scalable industrial applications.

An additional intermediate pyrolysis experiment was performed to validate the optimum conditions from simulations using the optimal parameters predicted by the PSO-ANFIS model of temperature, heating rate, residence time, particle size, and nitrogen flow rate of 510.2 °C, 10.5 °C/min, 5.2 min, 0.3 mm, and 17.3 mL/min, respectively. The bio-oil yield under these conditions was 51.54 wt.%, close to the predicted yield of 52.17 wt.%. The small deviation of 1.2% attests to the high predictive accuracy and reliability in predicting bio-oil yield with the PSO-ANFIS model. This experimental validation further reinforces the robustness of the hybrid optimization strategy for predicting and enhancing bio-oil yields in intermediate pyrolysis of *Cocos nucifera*.

3.8. Physicochemical Properties of the Bio-oil Sample

The physicochemical properties of bio-oil from *Cocos nucifera* pyrolysis show a pale brown colour, which suggests low carbonization, suitable for energy systems compared to darker oils requiring more treatment (Table 9). The bio-oil's acidic nature (pH 3.52) is close to that of fossil fuel, ranging from 4 to 6 in water-extraction fractions. Also, a high water content (21.7 wt.%) minimises the combustion performance in comparison to fossil fuels. Moreover, the bio-oil heating value (20.24 MJ/kg) is lower than that of diesel (42–45 MJ/kg) but lies in the range of some biomass fuels such as raw pyrolysis oils (16–24 MJ/kg), though the bio-oil retains a reasonable heating value of 20.24 MJ/kg, making it a feasible biofuel with potential upgrades needed for optimal performance. The density (1.13 g/cm^3) indicates good energy content per unit volume. The iodine value (49.4 mgKOH/g) shows moderate unsaturation, impacting oxidation stability. High viscosity (30.1 CST at 40°C) poses challenges for atomization and combustion, necessitating heating or blending with lighter oils. The bio-oil's elemental composition includes fair carbon (56.8 wt.%) and hydrogen (7.98 wt.%) content, enhancing energy density. Low nitrogen (0.21 wt.%) and sulfur (0.02 wt.%) levels reduce NOx emissions and corrosion risks. The bio-oil's flash point (88°C) indicates flammability at relatively low temperatures, posing a fire hazard during storage and transport. Conversely, the pour point (-10°C) ensures fluidity in cold environments, facilitating easier handling. Its low cetane index (20) reflects poor ignition quality compared to diesel (typically above 40), requiring modifications or blending for use in diesel engines. The Conradson carbon residue (10 wt.%) suggests a moderate level of combustion residue, indicating potential fouling in systems, though manageable with routine maintenance (Yuan *et al*., 2022).

Compared to fossil fuels, petroleum-derived fuels mainly comprise oxygen-free compounds, hydrocarbons like alkanes, cycloalkanes, and aromatics, with traces of oxygenated compounds. These fuels have a high proportion of hydrocarbons with little to no oxygen, making them more energy-dense and stable, unlike bio-oil, which is significantly different from conventional fossil fuels as its phenolics and fatty acids are oxygen-rich. The quality of the bio-oil yield could be improved by utilising several upgrading techniques. Catalytic upgrading via hydrodeoxygenation and zeolite cracking minimizes oxygen and boosts heating value, stability, and fuel compatibility with conventional fuel systems. Emulsification, formed by blending surfactants between diesel fuel and bio-oil, improves fuel combustion efficiency and stability in storage. Esterification and transesterification deacidify the bio-oil and reduce its corrosiveness to make the bio-oil more useful for engine applications. Fractional distillation also cleanses the biofuel by eliminating light and heavy fractions, improving its

Table 9
Characterisation of Bio-oil Yields at Optimum Operating Condition

Properties	***Cocos nucifera***
Appearance	Pale brown
pH	3.52
Water content (wt.%)	21.7
Density (g/cm^3)	1.13
Iodine value (mgKOH/mg)	49.4
Viscosity @ 40^{0}C (CST)	30.1
Carbon (wt.%)	56.8
Hydrogen (wt.%)	7.98
Nitrogen (wt.%)	0.21
Sulphur (wt.%)	0.02
Oxygen (wt.%)	26.23
HHV (MJ/kg)	20.24
Flash point	88
Pour point	-10
Cetane index	20
Conradson carbon residue (wt.%)	10.0

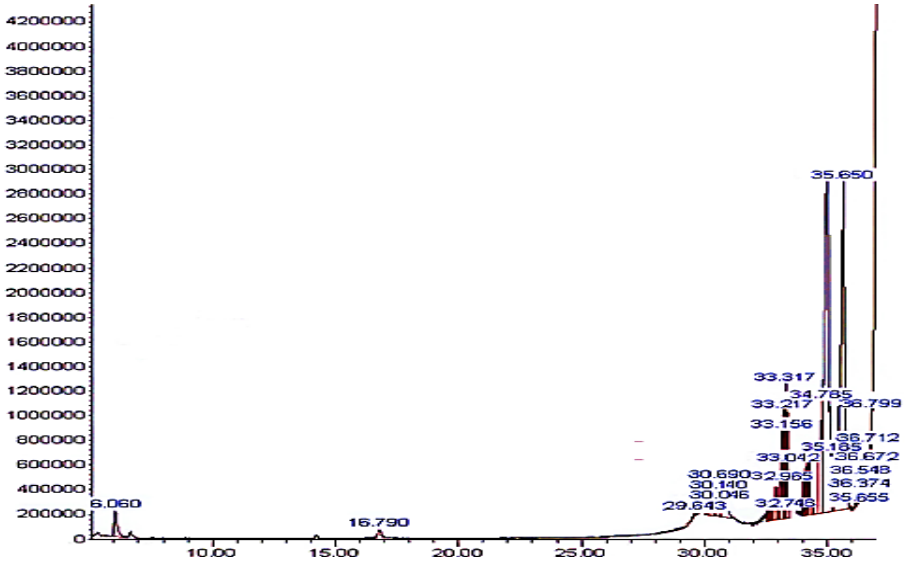

Fig 10. GC-MS of bio-oil compound

Table 10
Chemical composition of bio-oil yield using GC-MS analysis

S/N	Retention time (min)	Compound Name	Formula	Molecular Weight	Area wt.%
1	6.060	Phenol	C_6H_6O	94.0	1.65
2	16.788	9,12-octadecadienal	$C_{18}H_{32}O$	246.4	0.04
3	29.643	1,1-dimethyl-2-(2-propenyl) cyclopropane	C_8H_{14}	94.0	0.03
4	30.046	11-(2-Cyclopenten-1-yl) undecanoic acid	$C_{16}H_{28}O_2$	252.39	0.32
5	30.140	Oleic acid	$C_{18}H_{34}O_2$	264.0	0.62`
8	30.690	Oleic acid	$C_{18}H_{34}O_2$	264.0	2.76
9	32.748	Oleic acid	$C_{18}H_{34}O_2$	264.0	0.65
10	32.965	Oleic acid	$C_{18}H_{34}O_2$	264.0	1.14
11	33.042	9-Octadecenal	$C_{18}H_{34}O$	248.0	1.49
12	33.156	Cyclopentaneundecanoic acid	$C_{16}H_{30}O_2$	211.0	3.22
13	33.217	Oleic acid	$C_{18}H_{34}O_2$	264.0	2.66
14	33.251	Oleic acid	$C_{18}H_{34}O_2$	264.0	0.91
15	33.270	Oleic acid	$C_{18}H_{34}O_2$	264.0	1.46
16	33.317	Oleic acid	$C_{18}H_{34}O_2$	264.0	6.05
17	34.334	9,12-octadecadienoyl chloride	$C_{18}H_{31}ClO$	264.0	0.63
18	34.408	Oleic acid	$C_{18}H_{34}O_2$	264.0	0.61
19	34.560	Oleic acid	$C_{18}H_{34}O_2$	264.0	1.77
20	34.789	Oleic acid	$C_{18}H_{34}O_2$	264.0	6.01
21	34.957	9-oxabicyclo (6,1,0) nonane	$C_8H_{14}O$	126.0	28.84
22	35.185	9,12-octadecadienoyl chloride	$C_{18}H_{31}ClO$	264.0	2.02
23	35.655	9,12-octadecadienoyl chloride	$C_{18}H_{31}ClO$	264.0	27.46
24	36.374	9-oxabicyclo[6.1.0] nonane	$C_8H_{14}O$	126.19	0.04
25	36.548	9,17-octadecadienal	$C_{18}H_{32}O_2$	216.16	0.01
26	36.672	Oleic acid	$C_{18}H_{34}O_2$	264.0	0.07
27	36.712	Oleic acid	$C_{18}H_{34}O_2$	264.0	0.15
28	36.799	Oleic acid	$C_{18}H_{34}O_2$	264.0`	0.01

properties, and removing unwanted constituents. Also, solvent addition, such as mixing with ethanol or methanol, lowers viscosity, improves fluidity, and improves ignition quality, thereby making bio-oil a superior alternative fuel.

3.9. GC-MS analysis for Bio-oil

The chemical composition of bio-oil from *Cocos nucifera* pyrolysis was analyzed using GC-MS analysis. The spectrum, shown in Figure 10 and Table 10, identified over 200 compounds, with major components highlighted for peak areas above 0.5 wt.%. Key compounds include phenol (23.82 wt.%), oleic acid (32.22 wt.%), 9,17-octadecadienoyl (25.72 wt.%), and 9,12-octadecadienoyl chloride (7.09 wt.%). These compounds have significant industrial applications, such as phenol for Bisphenol-A, resins, and adhesives, while oleic acid is used for bio-lubricants, dyes, and therapeutics. The compounds Bisphenol-A, resins, adhesives, and oleic acid have vital economic value within different industries. Bisphenol-A is mainly utilised in polycarbonate plastics and epoxy resins, contributing about $8 billion to the market due to its use in the automobile, construction, and electronic industries. Resins and Adhesives are widely used in the industry for coatings, packaging, and industrial adhesives, contributing about $60 billion to industrial sectors. Likewise, Oleic acid is essential in the bio-lubricants, dye, and therapeutics industry for bio-enhancing, improving dye and pharmaceutical excipients, as it

contributes over $3 billion. Also, the fatty acids are helpful in treatment as anti-inflammatories and cholesterol-lowering agents. The industries' innovation and shift to biobased alternatives greatly depend on these compounds (Pang *et al.*, 2008). Methyl esters, known for their eco-friendly properties, find use in textiles and graphic arts. Ketones have broad applications in the medical, textiles, plastics, and cosmetics industries (Simonsen *et al.*, 2024). The presence of hydrocarbons, fatty acids, alcohols, esters, phenolics, and ketones indicates the bio-oil's potential as a renewable energy source, suitable for turbines, diesel engines, marine equipment, and industrial machinery. Additionally, phenol and methyl esters derived from lignin decomposition offer sustainable sources for adhesives, resins, and industrial products (Ma & Chen, 2024). The bio-oil's composition supports applications in energy, automotive, and pharmaceutical industries, underscoring its versatility and utility as a renewable resource (Jitpinit *et al.*, 2024). The versatility of bio-oil goes far beyond simply being used for fuel due to the presence of oxygenated compounds like phenolics and fatty acids. These compounds rich in oxygen increase bio-oil's usefulness in other industries like that as bio-lubricants, and even in pharmaceuticals as excipients. While petroleum fuels are mostly hydrocarbons, bio-oil provides a different chemical composition that is fundamental to sustainable energy and green chemistry. However, further refinement and catalytic upgrading processes are needed to enhance its stability and energy efficiency for use as a replacement drop-in fuel.

FTIR analysis of bio-oil from Cocos nucifera pyrolysis (500–4000 cm^{-1}) identified functional groups linked to its chemical composition (Table 11). Figure 11 shows the spectra, and Table 11 provides details on wavenumber ranges, observed peaks, corresponding molecular motions, and relative transmittance intensities to explain the bio-oil's chemical makeup. The dominant functional group identified is the hydroxyl group (O–H stretch) at 3389.2 cm^{-1}, indicating the presence of alcohols and phenols, which are typically byproducts of cellulose and hemicellulose breakdown in lignocellulosic biomass. The broad, strong appearance of this band confirms the prevalence of hydroxyl groups in bio-oils, as supported by previous studies (Rasheed *et al.,* 2023; Salim *et al.,* 2021; Kim *et al.,* 2020). The decarboxylation products released during pyrolysis are also suggested by the sharp absorption peak at 2400.4 cm^{-1}, which indicates carbon dioxide (O=C=O) stretching. Additionally, a notable peak at 2079.9 cm^{-1} corresponds to isothiocyanate (N=C=S stretching) groups, which may originate from proteinaceous compounds or nitrogen-containing materials within the biomass feedstock (Zou *et al.,* 2023). The C-H bending peak of aromatic hydrocarbons appears at 1766.8 cm^{-1}, contributing to the thermal stability and energy density of the bio-oil. Moreover, the presence of amines (N-H bending) at 1638.8 cm^{-1} signifies nitrogen functionalities likely formed through the thermal breakdown of nitrogenous organic matter. Phenolic groups are identified at 1349.3 cm^{-1} due to O-H bending vibrations, which are vital for the bio-oil's adhesive and resin properties. The

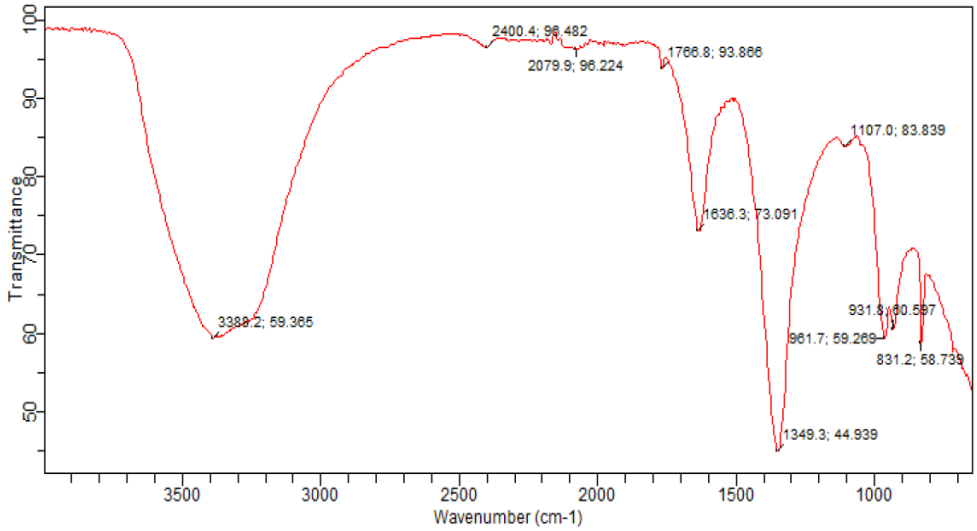

Fig 11. FT-IR spectrum of bio-oil yield

Table 11
Functional group composition of bio-oil yield

Functional Group	Wavenumber (cm^{-1})		Molecular Motion	wt.% Transmittance	Appearance
	Range	Actual			
Alcohol	2900-3700	3389.2	O-H stretching	59.385	Strong broad
Carbon dioxide	2350-2450	2400.4	O=C=O stretching	98.482	Strong broad
Isothiocyanate	2050-2150	2079.9	N=C=S stretching	98.224	Strong broad
Aromatic compound	1750-1790	1766.8	C-H bending	93.866	Weak broad
Amine	1550-1750	1638.8	N-H bending	73.091	Medium broad
Phenol	1150-1570	1349.3	O-H bending	44.939	Medium broad
Secondary Alcohol	1080-1150	1107.0	C-O stretching	83.839	Strong broad
Alkene	950-1060	961.7	C=C bending	59.289	Strong broad
Alkene	900-950	931.8	C=C bending	60.597	Strong broad
Halo compound	800-850	831.2	C-Cl stretching	58.739	Strong broad

secondary alcohol C-O stretching peak at 1107.0 cm^{-1} further confirms oxygenated compounds in the bio-oil. Alkene presence is indicated by C=C bonds at 961.7 and 931.8 cm^{-1}, suggesting unsaturated hydrocarbon chains that could enhance the oil's fuel potential. The C-Cl stretching peak at 831.2 cm^{-1} points to halogenated compounds, which, although present in smaller amounts, should be monitored due to environmental concerns when burned. Overall, the FTIR spectrum shows that the bio-oil contains rich oxygenated, nitrogenated, and hydrocarbon compounds derived from the thermochemical conversion of coconut biomass. These results support its potential use in energy production, pharmaceuticals, adhesives, and specialized chemical industries (Karacor & Özcanlı, 2024; Roy *et al.,* 2023)

The bio-oil yield from coconut shell (52.17 wt.%) is mid-to-high in comparison with other biomass sources, as demonstrated in Table 12. This value exceeds rice husk yields (38.13 wt.% and 47 wt.%), sugarcane bagasse (46.7 wt.%), and is similar to the bio-oil yields from baobab wood (52.70 wt.%) and Napier grass (50.57 wt.%). However, it is less than the optimum yields attained for Swietenia macrophylla (69.5 wt%) and co-pyrolysis of palm kernel shell and medical bottle (65.93 wt%). The presence of over 200 compounds, such as phenolic, ester, and oleic acid, makes the bio-oil yield from coconut shell more suitable for biofuels, lubricants, and pharmaceuticals. Its effective chemical composition and favourable functional groups, as evidenced by GC-MS and FTIR analyses, depict the bio-oil utilisation for advanced industrial applications, resin, and adhesive.

The bio-oil yield in this study is significantly better than fossil fuels. Studies showed that coconut biomass can contribute to an energy system that is more sustainable due to its being a renewable resource (Agrizzi *et al*., 2024; Azeta *et al*., 2021). In this study, agricultural residue was transformed into liquid fuel through intermediate pyrolysis under optimised conditions to improve the bio-oil yield, potentially mitigating environmental concerns connected to coconut waste. Results obtained from the physicochemical, FTIR, and GC-MS analysis of the bio-oil showed a substantial decrease in greenhouse gas emissions compared to fossil fuels. The carbon emitted during bio-oil combustion is captured as carbon dioxide by coconut trees during their growth, leading to a near-neutral carbon cycle. Also, bio-oil combustion generally results in low emissions of dangerous pollutants like sulphur dioxide and particulate matter as compared to fossil fuels.

4. Conclusions

The present study on intermediate pyrolysis of *Cocos nucifera* presents an improvement in biomass conversion technology by precisely optimizing operational parameters to achieve maximum yield of bio-oil using RSM. Performance metrics of different statistical parameters for bio-oil prediction models were carried out using RSM and hybrid models such as PSO-ANFIS and GA-ANFIS. Optimum conditions for the maximum bio-oil yield (52.17 wt.%) were found at a temperature of 501°C, a heating rate of 30°C/min, a residence time of 20 minutes, a particle size of 0.5 mm, and a nitrogen flow rate of 30 mL/min. These findings underscore the study's novel approach of balancing yield and product quality. The bio-oil produced is rich in valuable compounds such as phenols and oleic acids, which are suitable for biofuels, lubricants, and pharmaceuticals. This study advances prior research by integrating five pyrolysis operating parameters, such as temperature, heating rate, residence time, particle size, and nitrogen flow rate, into a comprehensive modelling framework, unlike previous studies, which only considered a few parameters. It utilises a new machine-learning hybrid model that integrates RSM with PSO-ANFIS and GA-ANFIS, significantly enhancing predictive accuracy and enabling real-time process control. The PSO-ANFIS and GA-ANFIS models accurately predict the bio-oil yield, with the PSO-ANFIS model outperforming the other models with an R^2 of 0.994 and RMSE of 0.449 during the test phase, representing a two- to three-fold improvement over traditional RSM. Moreover, the advanced hybrid models reduce time and cost by decreasing the number of experimental runs required while offering scalable applicability to diverse biomass feedstocks, especially in emerging economies. The results show that machine learning models combined with experimental data outperform RSM, which fails to capture complex nonlinear relationships. This makes the approach more suitable for large-scale biofuel production and industrial applications. This study is highly relevant for improving waste-to-energy production in regions where *Cocos nucifera* residues remain abundant, such as Nigeria. Further research should integrate this bio-oil into industrial applications as well as their long-term environmental impacts. Expanding to other biomass sources and including life-cycle assessment and catalytic pyrolysis will further validate such models and optimise the quality of the bio-oil yields for industrial applications. This work, therefore, provides the basis for the sustainable use of biomass, with reduced dependence on fossil fuels, toward the solution of global energy-environmental problems.

References

Abatyough, M. T., Ajibola, V. O., Agbaji, E. B., & Yashim, Z. I. (2022). Properties of upgraded bio-oil from pyrolysis of waste corn cobs. *Journal of Sustainability and Environmental Management*, *1*(2), 120–128. https://doi.org/10.3126/josem.v1i2.45348.

Abatyough, M., Ajibola, V. O., Agbaji, E. B., & Yashim, Z. (2022). Optimization of reaction conditions for bio-oil production from pyrolysis of corncobs. *Journal Of Chemical Society Of Nigeria,* 47(2). https://doi.org/10.46602/jcsn.v47i2.728

Abbasi, S., & Diwekar, U. M. (2014). Characterization and stochastic modeling of uncertainties in the biodiesel production. *Clean Technologies and Environmental Policy,* 16(1), 79–94. https://doi.org/10.1007/S10098-013-0596-4

Abonyi, M. N., Nwabanne, J. T., Ohale, P. E., Nwadike, E. C., Igbonekwu, L. I., Chukwu, M. M., & Madiebo, E. M. (2023). Application of RSM and ANFIS in the optimal parameter evaluation for crude oil degradation in contaminated water amended with PES. *Case Studies in Chemical and Environmental Engineering*, *8*, 100483. https://doi.org/10.1016/j.cscee.2023.100483

Afrah, B. D., Riady, M. I., Arsadha, J. P., Rimadhina, R., Cundari, L., & Izzah, R. Z. (2024). Effect of Pyrolysis Temperature and Biomass Composition on Bio-Oil Characteristics. *Ecological Engineering & Environmental Technology*, *25*. https://doi.org/10.12912/27197050/181152

Agrizzi, T., Oliveira, M. A., Faria, E. V., Santos, K. G., Xavier, T. P., & Lira, T. S. (2024). Assessing coconut shell pyrolysis: Biomass characterization, activation energy estimation, and statistical analysis of operating conditions. *Bioresource Technology Reports*, *26*, 101831. https://doi.org/10.1016/j.biteb.2024.101831

Agu, C. M., Ani, K. A., Ani, O. N., Nnaji, P. C., Kadurumba, C. H., & Esonye, C. (2024). Application of efficient soft computing approaches for modeling methyl ester yield from Azadirachta Indica (Neem) seed oil: A comparative study of RSM, ANN and ANFIS. *Green Technologies and Sustainability*, *2*(1), 100057. https://doi.org/10.1016/j.grets.2023.100057

Ahmad, R. K., Sulaiman, S. A., Dol, S. S., & Umar, H. A. (2021). The Potential of Coconut Shells Through Pyrolysis Technology in Nigeria. In S. A. Sulaiman (Ed.), *Clean Energy Opportunities in*

Tropical Countries (pp. 151–175). Springer Singapore. https://doi.org/10.1007/978-981-15-9140-2_8

Ahmed, A., Harun, N. Y., Waqas, S., Arshad, U., & Ghalib, S. A. (2024). Optimization of Operational Parameters Using Artificial Neural Network and Support Vector Machine for Bio-oil Extracted from Rice Husk. *ACS Omega,* 9(24), 26540–26548. https://doi.org/10.1021/acsomega.4c03131

Akuwueke, L. M., Ossia, C. V., and Nwosu, H. U. (2024). Proximate Property and Thermal Stability Characterization of Chemically Activated Carbon for Organic Friction Lining Materials. *Nigerian Journal of Technology*, 43(3), pp. 454 – 463. https://doi.org/10.4314/njt.v43i3.7

ASTM International. (2021). Standard test method for acid-insoluble lignin in wood (ASTM Standard No. D1106-21). ASTM International.

ASTM International. (2002). Standard test method for moisture in the analysis sample of coal and coke (ASTM Standard No. D3173-02). ASTM International.

ASTM International. (2011). Standard test method for ash in the analysis sample of coal and coke from coal (ASTM Standard No. D3174-02(2011)). ASTM International.

ASTM International. (2020). Standard test method for volatile matter in the analysis sample of coal and coke (ASTM Standard No. D3175-20). ASTM International.

ASTM International. (2011). Standard test method for sulfur in the analysis sample of coal and coke using high-temperature tube furnace combustion (ASTM Standard No. D4239-11). ASTM International.

ASTM International. (2016). Standard test method for determination of carbon, hydrogen, and nitrogen in analysis samples of coal and carbon in analysis samples of coal and coke (ASTM Standard No. D5373-16). ASTM International.

ASTM International. (2013). Standard test method for gross calorific value of coal and coke (ASTM Standard No. D5865-13). ASTM International.

ASTM International. (2013). Standard practice for general techniques for obtaining infrared spectra for qualitative analysis (ASTM Standard No. E1252-98(2013)). ASTM International.

ASTM International. (2020). Standard test method for determination of carbohydrates in biomass by high performance liquid chromatography (ASTM Standard No. E1758-01(2020)). ASTM International

Azeta, O., Ayeni, A. O., Agboola, O., & Elehinafe, F. B. (2021). A review on the sustainable energy generation from the pyrolysis of coconut biomass. *Scientific African*, *13*, e00909. https://doi.org/10.1016/j.sciaf.2021.e00909

Azizi, M. W., Bensouici, M., & Bensouici, F. Z. (2024). Thermoexergetic analysis and multi-objective optimization of steam power plant performances. *AIUB Journal of Science and Engineering (AJSE)*, *23*(2), 124–134. https://doi.org/10.53799/ajse.v23i2.909

Berggren, M. (2023). *Coefficients of determination measured on the same scale as the outcome*. https://doi.org/10.31234/osf.io/svuf8

Chhikara, A., Dhingra, A. K., & Kumar, P. (2023). Improvement and Optimisation of Castor Oil Bio-diesel Using RSM and ANN-GA (pp. 257–272). *Springer Nature*. https://doi.org/10.1007/978-981-99-1308-4_21

Chan, Y. H., Yusup, S., Quitain, A. T., Uemura, Y., & Loh, S. K. (2017). Fractionation of pyrolysis oil via supercritical carbon dioxide extraction: Optimization study using response surface methodology (RSM). *Biomass & Bioenergy,* 107, 155–163. https://doi.org/10.1016/J.BIOMBIOE.2017.10.005

Chantarangsi, W., Liu, W., Bretz, F., Kiatsupaibul, S., Hayter, A. J., & Wan, F. (2015). Normal probability plots with confidence. *Biometrical Journal*, *57*(1), 52–63. https://doi.org/10.1002/bimj.201300244

Chen, X., Pei, Y., Wang, X., Zhou, W., & Jiang, L. (2024). Response Surface Methodology—Central Composite Design Optimization Sugarcane Bagasse Activated Carbon under Varying Microwave-Assisted Pyrolysis Conditions. *Processes*, *12*(3), 497. https://doi.org/10.3390/pr12030497

Chukwuneke, J. L., Sinebe, J. E., Orugba, H. O., & Ajike, C. (2022). Process Optimization for Enhancing Yield and Quality of Bio-Oil from the Pyrolysis of Cow Hooves. I*nternational Journal of Design & Nature and Ecodynamics,* 17(3), 453–461. https://doi.org/10.18280/ijdne.170317

Chukwuneke, J. L., Ewulonu, M. C., Chukwujike, I. C., & Okolie, P. C. (2019). Physico-chemical analysis of pyrolyzed bio-oil from swietenia macrophylla (mahogany) wood. *Heliyon*, *5*(6). https://doi.org/10.1016/j.heliyon.2019.e01790

Cuevas, E., Ascencio-Piña, C. R., Pérez, M., & Morales-Castañeda, B. (2024). Considering radial basis function neural network for effective solution generation in metaheuristic algorithms. *Scientific Reports*, *14*(1), 16806. https://doi.org/10.1038/s41598-024-67778-0

Di Lauro, F., Amadei, A., Balsamo, M., Damizia, M., de Caprariis, B., De Filippis, P., Solimene, R., Salatino, P., & Montagnaro, F. (2024). Effect of the reactor heating rate on bio-crude yield and quality from hydrothermal liquefaction of different sludge. *Fuel Communications*, *19*, 100113. https://doi.org/10.1016/j.jfueco.2024.100113

Djandja, O. S., Salami, A. A., Yuan, H., Lin, H., Huang, Z., & Kang, S. (2023). Machine learning prediction of bio-oil yield during solvothermal liquefaction of lignocellulosic biowaste. *Journal of Analytical and Applied Pyrolysis*. https://doi.org/10.1016/j.jaap.2023.106209

Garg, A., Basu, S., Shetti, N. P., Bhattu, M., Alodhayb, A., & Pandiaraj, S. (2024). Biowaste to bioenergy nexus: Fostering sustainability and circular economy. *Environmental Research*, 118503. https://doi.org/10.1016/j.envres.2024.118503

Haq, Z. U., Ullah, H., Khan, M. N. A., Naqvi, S. R., Ahad, A., & Amin, N. A. S. (2022). Comparative study of machine learning methods integrated with genetic algorithm and particle swarm optimization for biochar yield prediction. *Bioresource Technology*, *363*, 128008. https://doi.org/10.1016/j.biortech.2022.128008

Hasan, M. M., Rasul, M. G., Jahirul, M. I., & Khan, M. M. K. (2023). Fast pyrolysis of macadamia nutshell in an auger reactor: Process optimization using response surface methodology (RSM) and oil characterization. *Fuel*, *333*, 126490. https://doi.org/10.1016/j.fuel.2022.126490

Hassan, H., Ahmad, M. A., Zali, N. D. A., Musa, M. Z., & Senusi, F. (2024). Co-pyrolysis of palm kernel shell and discarded medical bottle for biofuel production: Synergistic effect and product distribution. *Waste Management Bulletin*, *1*(4), 182–194. https://doi.org/10.1016/j.wmb.2023.11.001

Hassan, S. N., Ishak, M. A., & Ismail, K. (2019). Optimizing the physical parameters to achieve maximum products from co-liquefaction using response surface methodology. *Fuel,* 207, 102–108. http://dx.doi.org/10.1016/j.fuel.2017.06.077

Huang, D., Wang, Y., Song, G., Hu, S., Li, H., Zhang, Y., Wang, Y., Su, S., El-Sayed, S. A., & Xiang, J. (2023). Study on thermal properties of biochar prepared by photo-thermal pyrolysis. *Biomass and Bioenergy*, *178*, 106969. http://dx.doi.org/10.3390/en10040469

Huraira, M. M., Saravanathamizhan, R., Israel, T. T., Haripriyan, U., & Perarasu, V. T. (2023). Modeling and optimization of the yield of pyrolytic oil from waste face masks using RSM-ANN-LM hybrid approach. *Environmental Quality Management.* https://doi.org/10.1002/tqem.22133

Ikpeseni, S. C., Sada, S. O., Efetobor, U. J., Orugba, H. O., Ekpu, M., Owamah, H. I., Chukwuneke, J. L., Oyebisi, S., & Onochie, U. P. (2024). Optimization of bio-oil production parameters from the pyrolysis of elephant grass (Pennisetum purpureum) using response surface methodology. *Clean Energy*, *8*(5), 241–251. https://doi.org/10.1093/ce/zkae064

Jabeen, S., Baig, M., & Awais, M. M. (2023). ANFIS learning using expectation maximization based Gaussian mixture model and multilayer perceptron learning. *Applied Soft Computing*, *149*, 110958. https://doi.org/10.1016/j.asoc.2023.110958

Jalalifar, S. (2020). *Operational management of fast pyrolysis process using numerical modelling* [PhD Thesis, University of Tasmania]. https://doi.org/10.25959/100.00035036
https://figshare.utas.edu.au/articles/thesis/Operational_management_of_fast_pyrolysis_process_using_numerical_modelling/23253788/1

Jalalinejad, A., Yousefi Seyf, J., Funke, A., & Dahmen, N. (2024). Phase Equilibrium Calculation of Bio-Oil-Related Molecules Using Predictive Thermodynamic Models. *Energy & Fuels*, *38*(4), 3171–3185. https://doi.org/10.1021/acs.energyfuels.3c04395

Jitpinit, S., Chisti, Y., Rattanasak, U., Rakmak, N., & Nuithitikul, K. (2024). Hydrothermal liquefaction of oil-palm-derived lignin to bio-oils for use as antioxidants in biodiesel. *Journal of Industrial*

and Engineering Chemistry, *135*, 243–256. http://dx.doi.org/10.1016/j.jiec.2024.01.036

Karacor, B., & Özcanlı, M. (2024). A Short Review: The Use and Application of Matrix Resins Formed with Some Plant-Based Oils in Bio-Composite Materials. *Düzce Üniversitesi Bilim ve Teknoloji Dergisi*, *12*(3), 1315–1333. https://doi.org/10.29130/dubited.1265905

Kaur, L., Singh, J., Ashok, A., & Kumar, V. (2024). Design expert based optimization of the pyrolysis process for the production of cattle dung bio-oil and properties characterization. *Dental Science Reports*, 14(1), 9421. https://doi.org/10.1038/s41598-024-57843-z

Kim, J. S., & Park, K. B. (2020). Production of Phenols by Lignocellulosic Biomass Pyrolysis (pp. 289–319). Springer, Singapore. https://doi.org/10.1007/978-981-15-2732-6_11

Kozak, M., & Piepho, H. -P. (2018). What's normal anyway? Residual plots are more telling than significance tests when checking ANOVA assumptions. *Journal of Agronomy and Crop Science*, *204*(1), 86–98. https://doi.org/10.1111/jac.12220

Kumar, M., Mishra, P. K., & Upadhyay, S. N. (2019). Pyrolysis of Saccharum munja: Optimization of process parameters using response surface methodology (RSM) and evaluation of kinetic parameters. *Bioresource Technology Reports*, *8*, 100332. https://doi.org/10.1016/j.biteb.2019.100332

Kumar, S., & Bansal, S. (2023). Performance evaluation of ANFIS and RSM in modeling biodiesel synthesis from soybean oil. *Biosensors and Bioelectronics: X*, *15*, 100408. https://doi.org/10.1016/j.biosx.2023.100408

Kundu, R., Parsad, R., & Mandal, B. N. (2024). Response surface designs with four and six equi-spaced levels. *Communications in Statistics - Theory and Methods*, 1–14. https://doi.org/10.1080/03610926.2024.2423816

Laougé, Z. B., Çığgın, A. S., & Merdun, H. (2020). Optimization and characterization of bio-oil from fast pyrolysis of Pearl Millet and Sida cordifolia L. by using response surface methodology. *Fuel*, *274*, 117842. http://dx.doi.org/10.1016/j.fuel.2020.117842

Li, Z., Zhao, D., Han, L., Yu, L., & Jafari, M. M. M. (2021). Improved Estimation of Bio-Oil Yield Based on Pyrolysis Conditions and Biomass Compositions Using GA- and PSO-ANFIS Models. *BioMed Research International*, *2021*, 1–9. https://doi.org/10.1155/2021/2204021

Ma, H., & Chen, D. (2024). Direct conversion of lignin to liquid hydrocarbons for sustainable biomass valorization. *Catalysis Today*, *441*, 114882. https://doi.org/10.1016/j.cattod.2024.114882

Mathur, J., Baruah, B., & Tiwari, P. K. (2022). Prediction of Bio-Oil yield during pyrolysis of lignocellulosic biomass using Machine Learning Algorithms. *Canadian Journal of Chemical Engineering*, 101(5), 2457–2471. https://doi.org/10.1002/cjce.24674

Mbah, C., Nwafulugo, F., & Ezetoha, N. (2024). Comparism of Response Surface Methodology (RSM) and Adaptive Neuro-Fuzzy Inference Systems (ANFIS) in Optimisation of Soybean Soapstock Biodiesel Production. *Advances*, *5*(2), 49–63. https://doi.org/10.11648/j.advances.20240502.13

Mian, I., Rehman, N., Li, X., Ullah, H., Khan, A., Choi, C., & Han, C. (2024). Effect of Heating Rate on the Pyrolysis Behavior and Kinetics of Coconut Residue and Activated Carbon: A Comparative Study. *Energies*, *17*(18), 4605. https://doi.org/10.3390/en17184605

Mohammed, I. Y., Abakr, Y. A., Yusup, S., & Kazi, F. K. (2017). Valorization of Napier grass via intermediate pyrolysis: Optimization using response surface methodology and pyrolysis products characterization. *Journal of Cleaner Production*, *142*, 1848–1866. https://doi.org/10.1016/j.jclepro.2016.11.099

Mwenge, P., Rutto, H., & Seodigeng, T. (2024). Modelling and Optimisation of Biodiesel Production from Margarine Waste Oil Using a Three-Dimensional Machine Learning Approach. 22, 27. https://doi.org/10.3390/engproc2024067027

Nawaz, A., Razzak, S. A., & Kumar, P. (2024). Pyrolysis parameter based optimization study using response surface methodology and machine learning for potato stalk. *Journal of the Taiwan Institute of Chemical Engineers*, *159*, 105476. http://dx.doi.org/10.1016/j.jtice.2024.105476

Okokpujie, I. P., Onokwai, A. O., Onokpite, E., Babaremu, K., Ajisegiri, E. S. A., Osueke, C. O., Akinlabi, S. A., & Akinlabi, E. T. (2023). Modelling and optimisation of intermediate pyrolysis synthesis of bio-oil production from palm kernel shell. *Cleaner Engineering and Technology*, *16*, 100672. https://doi.org/10.1016/j.clet.2023.100672

Olayokun, O. E., Anyaegbuna, B. E., Onokwai, A. O., Faola, D. I., Muslim, I. O., Eruobodo, A. O., & Adiatu, A. O. (2024). Review of Biomass as a Renewable Energy for Sustainable Environment. *2024 International Conference on Science, Engineering and Business for Driving Sustainable Development Goals (SEB4SDG)*, 1–7. http://dx.doi.org/10.1109/SEB4SDG60871.2024.10629775

Onochie, U. P., Ofomatah, A. C., Onwurah, C., Tyopine, A. A., Akingba, O. O., Kubeynje, B. F., Aluma, C. C., Alozie, C. (2023). Potentials of Biomass Waste Resources with Respect to their Calorific Value, Proximate and Ultimate Analysis for Energy Utilization. *IOP Conf. Series: Earth and Environmental Science*, 1178, 012012, IOP https://doi.org/10.1088/1755-1315/1178/1/012012

Onokwai, A. O., Akuru, U. B., & Desai, D. A. (2025). Mathematical Modelling and Optimisation of Operating Parameters for Enhanced Energy Generation in Gas Turbine Power Plant with Intercooler. *Mathematics*, *13*(1), 174. https://doi.org/10.3390/math13010174

Onokwai, A. O., Okokpujie, I. P., Ajisegiri, E. S. A., Nnodim, C. T., Kayode, J. F., & Tartibu, L. K. (2024). Application of response surface methodology for the modelling and optimisation of bio-oil yield via intermediate pyrolysis process of sugarcane bagasse. *Advances in Materials and Processing Technologies*, *10*(4), 3028–3046. https://doi.org/10.1080/2374068X.2023.2193310

Onokwai, A. O., Okokpujie, I. P., Ajisegiri, E. S., Oki, M., Adeoye, A. O., & Akinlabi, E. T. (2022). Characterization of Lignocellulosic Biomass Samples in Omu-Aran Metropolis, Kwara State, Nigeria, as Potential Fuel for Pyrolysis Yields. *International Journal of Renewable Energy Development*, *11*(4). https://doi.org/10.14710/ijred.2022.45549

Othman, P. S., Ihsan, R. R., & Abdulhakeem, R. M. (2022). The Genetic Algorithm (GA) in Relation to Natural Evolution. *Academic Journal of Nawroz University*, *11*(3), 243–250.

Oyebanji, J. A., Okekunle, P. O., Lasode, O. A., & Oyedepo, S. O. (2018). Chemical composition of bio-oils produced by fast pyrolysis of two energy biomass. *Biofuels*, *9*(4), 479–487. https://doi.org/10.1080/17597269.2017.1284473

Oyebanji, J. A., Onokwai, A. O., Okokpujie, I. P., Ukegbu, C. F., SuyiAjayi, A., Nnochiri, E. S., & Tartibu, L. K. (2023). Characterization of Adansonia Digitata (Baobab Wood) Bio-Oil and Biochar Produced Using a Fixed-Bed Tubular Reactor. *Journal of Composite & Advanced Materials/Revue Des Composites et Des Matériaux Avancés*, *33*(1). https://doi.org/10.18280/rcma.330208

Özbay, G., & Kokten, E. S. (2019). Modeling of Bio-Oil Production by Pyrolysis of Woody Biomass: Artificial Neural Network Approach. *Journal of Polytechnic,* 23(4), 1255–1264. https://doi.org/10.2339/POLITEKNIK.659136

Pang, Z. (2008). Production and Market Analysis of Bisphenol A. Chemical Industry. https://en.cnki.com.cn/Article_en/CJFDTOTAL-HGJJ200809009.htm

Prasetiawan, H., Hadiyanto, Fardhyanti, D. S., Fatriasari, W., Chafidz, A., Rakasiwi, A. G., Kaja, Y. V., Rahma, N. F., & Laili, I. R. (2023). Bio Oil Production from Multi-Feed Stock Biomass Waste and the Upgrading Process for Quality Improvement - Mini Review. *IOP Conference Series: Earth and Environmental Science*, *1203*(1), Article 012040. https://doi.org/10.1088/1755-1315/1203/1/012040

Rahimi, M., Mashhadimoslem, H., Thanh, H. V., Ranjbar, B., Khosrowshahi, M. S., Rohani, A., & Elkamel, A. (2023). Yield prediction and optimization of biomass-based products by multi-machine learning schemes: Neural, regression and function-based techniques. *Energy*, *283*, 128546. http://dx.doi.org/10.1016/j.energy.2023.128546

Rasheed, H. A., Ayuba, S., Adeleke, A., Ogedengbe, T. S., Nzerem, P., & Ikubanni, P. P. (2023). Compositional Analysis and Characterisation of Non-edible Plant Biomass for Carboxymethyl Cellulose Production. 1, 1–5. https://doi.org/10.1109/icmeas58693.2023.10379365

Ratnasari, R., Wardhani, G. A. P. K., & Taufiq, A. (2024). Bio-oil Quality Based on Coconut Carbon Biomass Using Pyrolisis Method.

Indonesian Journal of Chemical Research, *12*(2), 153–163. http://dx.doi.org/10.30598/ijcr.2024.12-rif

Roy, P., Rahman, T., Jackson, R. L., Jahromi, H., & Adhikari, S. (2023). Hydrocarbon biolubricants from hydrotreated renewable and waste derived liquid intermediates. *Journal of Cleaner Production*, *409*, 137120. https://doi.org/10.1016/j.jclepro.2023.137120

Salameh, T., Sayed, E. T., Olabi, A. G., Hdaib, I. I., Allan, Y., Alkasrawi, M., & Abdelkareem, M. A. (2022). Adaptive network fuzzy inference system and particle swarm optimization of biohydrogen production process. *Fermentation*, *8*(10), 483. https://doi.org/10.3390/fermentation8100483

Salim, R. M., Asik, J., & Sarjadi, M. S. (2021). Chemical functional groups of extractives, cellulose and lignin extracted from native Leucaena leucocephala bark. Wood Science and Technology, 55(2), 295–313. https://doi.org/10.1007/S00226-020-01258-2

Sareekam, N., Kamarudin, S. K., & Kasmuri, N. H. (2016). Optimization of Bio Oil from Palm Oil Fronds Via Fast Pyrolysis. *Indian Journal of Science and Technology,* 9(21), 95232. https://doi.org/10.17485/IJST/2016/V9I21/95232

Şener, R., Koç, M. A., & Ermiş, K. (2024). Hybrid ANFIS-PSO algorithm for estimation of the characteristics of porous vacuum preloaded air bearings and comparison performance of the intelligent algorithm with the ANN. *Engineering Applications of Artificial Intelligence*, *128*, 107460. https://doi.org/10.1016/j.engappai.2023.107460

Simonsen, T. I., Djajadi, D. T., Montanvert, H., Sgarzi, M., Gigli, M., Thomsen, S. T., Orozco, Y. C., & Crestini, C. (2024). Improving the production efficiency and sustainability of lignin-alcohol fuel processed at ambient temperature. *Bioresource Technology*, *408*, 131087. https://doi.org/10.1016/j.biortech.2024.131087

Tabal, A., Belyazid, O., Dahman, H., Berrich, E., Jeguirim, M., El Achaby, M., El Harfi, K., & Aboulkas, A. (2023). Intermediate pyrolysis of Ficus nitida wood in a fixed-bed reactor: Effect of pyrolysis parameters on bio-oil and biochar yields and properties. *Comptes Rendus. Chimie*, *26*(S1), 1–17. http://dx.doi.org/10.5802/crchim.253

Tang, Z., Li, L., & Pang, C. H. (2024). Review of Biomass Gasification and Pyrolysis Process Based on Long Short-Term Memory Network. *Applied and Computational Engineering*, *103*, 162–168. http://dx.doi.org/10.54254/2755-2721/103/20241158

Téllez, J. F., Silva, M. P., Simister, R., Gomez, L. D., Fuertes, V. C., De Paoli, J. M., & Moyano, E. L. (2021). Fast pyrolysis of rice husk under vacuum conditions to produce levoglucosan. *Journal of Analytical and Applied Pyrolysis*, *156*, 105105. http://dx.doi.org/10.1016/j.jaap.2021.105105

Titov, A. P. (2024). Analysis of models of adaptive neuro-fuzzy systems. Vestnik RGGU. Seriâ: Informatika. Informacionnaâ Bezopasnost'. *Matematika,* 1, 21–35. https://doi.org/10.28995/2686-679x-2024-1-21-35

Tumuluru, J. S., & Heikkila, D. J. (2019). Biomass grinding process optimization using response surface methodology and a hybrid genetic algorithm. *Bioengineering*, *6*(1), 12. https://doi.org/10.3390/bioengineering6010012

Vellaiyan, S., Chandran, D., Venkatachalam, R., Ramalingam, K., Rao, R., & Raviadaran, R. (2024). Maximizing waste plastic oil yield and enhancing energy and environmental metrics through pyrolysis process optimization and fuel modification. *Results in Engineering*, *22*, 102066. https://doi.org/10.1016/j.rineng.2024.102066

Wakatuntu, J., Olupot, P. W., Jjagwe, J., Menya, E., & Okure, M. (2023). Optimization of pyrolysis conditions for production of rice husk-based bio-oil as an energy carrier. *Results in Engineering*, *17*, 100947.

Wulandari, Y. R., Chen, S. S., Hermosa, G. C., Hossain, M. S. A., Yamauchi, Y., Ahamad, T., Alshehri, S. M., Wu, K. C., & Wu, H.-S. (2020). Effect of N2 flow rate on kinetic investigation of lignin pyrolysis. *Environmental Research*, *190*, 109976.

Xu, L., Jiang, L., Zhang, H., Fang, Z., & Smith, R. L. (2020). Introduction to Pyrolysis as a Thermo-Chemical Conversion Technology. In Z. Fang, R. L. Smith Jr, & L. Xu (Eds.), *Production of Biofuels and Chemicals with Pyrolysis* (Vol. 10, pp. 3–30). Springer Singapore. https://doi.org/10.1007/978-981-15-2732-6_1

Yi, Z., Li, C., Lin, H., Zhang, S., Huang, Y., Li, B., Wang, S., & Hu, X. (2023). Pyrolysis of sawdust impregnated with bio-oil of the same origin: Influence of organics in bio-oil on property of biochar. *Biomass and Bioenergy*, *178*, 106961.

Yuan, H., Tsukuda, T., Yang, Y., Shibata, G., Kobashi, Y., & Ogawa, H. (2022). Effects of chemical compositions and cetane number of Fischer–Tropsch fuels on diesel engine performance. *Energies*, *15*(11), 4047

Zhao, C., Lü, X., Jiang, Z., Ma, H., Chen, J., & Liu, X. (2024). Prediction of bio-oil yield by machine learning model based on "enhanced data" training. *Renewable Energy,* 225, 120218. https://doi.org/10.1016/j.renene.2024.120218

Zou, S., Lei, J., Gao, T., Xu, X., & Gou, Q. (2023). C···S Tetrel Bond Favored in the Phenyl Isothiocyanate-CO_2 Complex: A Rotational Study. *Journal of Physical Chemistry A*. https://doi.org/10.1021/acs.jpca.3c05187